LUT University

PRECISION TEMPERATURE MEASUREMENTS IN WEARABLES

Practical considerations

Lappeenranta-Lahti University of Technology LUT

Degree Programme in Electrical Engineering, Master's Thesis

2022

Otto Salminen

Examiners: Professor Pertti Silventoinen

Associate Professor Mikko Kuisma

Abstract

Lappeenranta-Lahti University of Technology LUT
LUT School of Energy Systems
Electrical Engineering

Otto Salminen

Precision temperature measurements in wearables
Practical considerations

Master's Thesis
2022

81 pages, 39 figures, 9 tables, 6 appendices.
Examiners: Professor Pertti Silventoinen and Associate Professor Mikko Kuisma

Keywords: Temperature sensors, wearables, biosignals

Wearable devices collect multiple measurements from the user and based on these calculate various metrics to be displayed. One of these metrics is energy expenditure which has been traditionally calculated using metabolism models and heart rate, typically having large error margins. Improved results have been achieved by augmenting the estimate with heat flux data measured from the subject, where accurate temperature measurements play a key role. The purpose of this thesis was to study suitable temperature sensors for wearable applications and to design a test setup for conducting measurements on their practical performance. This thesis was conducted for LUT university in collaboration with Vire Health Oy.

A literature review was conducted on the fundamentals of temperature measurement technologies and their suitability for this particular use case. Based on the literature review and previous experiences potential temperature sensor candidates were proposed for further study. Based on previous prototypes a summary of the used ADC functionalities and practical considerations was documented for future use.

A test setup was designed to examine the practical performance of the selected sensors and the ADC, modular circuit boards were made that could be used for this thesis and possible future measurements. Measurement parameters for the selected sensors and the ADC were proposed that would yield optimal results for initial measurements.

Based on the measurement results the variations between sensors from the same manufacturing batch can be large but predictable and they can be corrected by calibrating the sensors. Further tests are required to study the practical resolution limits of the sensors and ADC, in a more controlled environment where the effects of other personnel in the vicinity of the test setup can be mitigated and changes in the ambient environment can be controlled.

Tiivistelmä

Lappeenrannan-Lahden teknillinen yliopisto LUT
LUT Energiajärjestelmät
Sähkötekniikka

Otto Salminen

Tarkat lämpötilamittaukset puettavassa elektroniikassa
Käytännön huomioita

Diplomityö
2022

81 sivua, 39 kuvaa, 9 taulukkoa, 6 liitettä.
Tarkastajat: Professori Pertti Silventoinen ja tutkijaopettaja Mikko Kuisma

Hakusanat: Lämpötila-anturit, puettava elektroniikka, biosignaalit

Puettava elektroniikka mittaa käyttäjästään useita eri asioita ja laskee näiden mittausten perusteella erilaisia parametrejä, jotka kertova käyttäjän sen hetkisestä olotilasta. Yksi näistä mittareista on energiankulutus, joka perustuu tyypillisen ihmisen aineenvaihdunnan malliin sekä sykkeeseen. Tyypillisesti tällaisessa mittauksessa virhemarginaalit ovat suuria. Kokeellisissa mittauksissa virhettä on saatu pienennettyä yhdistämällä energiankulutusarvioon käyttäjästä mitattua lämpövuodataa, jonka tarkkuuteen vaikuttaa referenssilämpötilan mittauksen tarkkuus. Tutkimuksen päätavoitteena oli löytää tähän käyttöön sopivia lämpötila-antureita sekä suunnitella mittausjärjestely valittujen anturien käytännön suorituskyvyn mittaamiseen. Työ tehtiin LUT yliopistolle yhteistyössä Vire Health Oy:n kanssa.

Kirjallisuuskatsauksessa tutkittiin lämpötilan mittaamista sekä siihen soveltuvia teknologioita ja aikaisempien kokemusten sekä tämän tutkimuksen perusteella valittiin neljä sopivaa anturia jatkotutkimuksia varten. Aikaisemmissa prototyypeissä käytetyn A/D-muuntimen ominaisuudet ja käyttämisen kannalta oleelliset parametrit dokumentoitiin tulevia projekteja ajatellen.

Työssä suunniteltiin mittausjärjestelyt anturien sekä A/D-muuntimen suorituskyvyn mittaamiseen ja mittauksia varten suunniteltiin piirilevyt, joita voitaisiin käyttää myös mahdollisissa jatkotutkimuksissa. Antureille sekä A/D-muuntimelle on esitelty käytettävät mittausparametrit.

Mittausten perusteella anturien välillä voi olla suurtakin poikkeamaa valmistuserän sisällä, tosin nämä poikkeavuudet ovat ennustettavissa ja ne voidaan korjata kalibroimalla yksittäiset anturit. Jatkotutkimuksia tulee suorittaa anturien ja A/D-muuntimen käytännön resoluution tutkimiseksi tilassa, jossa ympäristön vaikutukset mittausjärjestelyihin ovat paremmin hallittavissa.

Acknowledgements

This master's thesis was conducted at LUT University for The Laboratory of Applied Electronics in collaboration with Vire Health Oy. The four years spent participating around the research subject of wearables, heat flux and human measurements has been fascinating.

I would like to express special thanks to my supervisors Prof. Pertti Silventoinen and Assoc. Prof. Mikko Kuisma for the topic, their guidance, and insightful feedback during the writing process. Without your support and expertise this thesis would not have been possible.

I wish to express my gratitude to the whole Skinnarila campus. The seven years spent participating in the activities of Norpparadio, Sätky and LTKY has brought me many new friends for life and memorable experiences not possible anywhere else.

Big thanks goes out for all of my colleagues who I have had the pleasure to work with at the university, both around my master's thesis and with other projects. Special thanks to Matias for helping me with the PCB manufacturing and assembly process when the schedule was tight, without your help none of my measurements could have been completed.

Finally I would like to thank my family for their support throughout my studies.

Jos kukaan ei suutu, mikään ei muutu,

Otto Salminen
Helsinki, June 8, 2022

Symbols and abbreviations

Roman characters

ΔT	Self heating temperature error	[K]
A	Contact area	[m^2]
E	Self heating coefficient	[mW/K]
f_c	Measurement cycle	[Hz]
h	Heat transfer coefficient	[W / m^2 K]
I	Excitation current	[mA]
$I_{AV_{DD}}$	Analogue power supply current	[A]
$I_{IO_{VDD}}$	Digital power supply current	[A]
k	Thermal conductivity	[W/K]
M_t	Thermal mass of the device and surrounding PCB area	[J/K]
$n_{sensors}$	Number of sensors	[1]
P_s	Average power dissipated	[W]
q	Heat flux	[W/m^2]
R	Resistance of the sensor	[kΩ]
R_{sa}	Thermal resistance between the sensor and the environment	[K/W]
R_{so}	Thermal resistance between the sensor and the object	[K/W]
T	Temperature	[K]
T_∞	Environment temperature	[K]
T_{air}	Environment temperature	[K]
T_f	Bulk fluid temperature	[K]
T_{obj}	Measured object temperature	[K]
t_{settle}	Filter settling time	[s]
T_s	Sensor temperature	[K]
T_s	Surface temperature	[K]
V_{OS}	Offset voltage	[V]
V_{out}	Output voltage	[V]
V_{ref}	Voltage reference	[V]
x	Distance	[m]

Greek characters

ϵ	Surface emissivity
σ	Stefan-Boltzmann constant

Abbreviations

$\Sigma - \Delta$	Sigma-Delta
ADC	Analogue-to-Digital converter
AV_{SS}	Analogue ground
DAS	Data acquisition system

DGND	Digital ground
DMM	Digital multimeter
DUT	Device under test
EE	Energy expenditure
EEPROM	Erasable programmable read-only memory
EMF	Electromotive force
GPIO	General purpose input/output
HF	Heat flux
I^2C	Inter-integrated circuit
I/O	Input/Output
IC	Integrated circuit
IPRT	Industrial platinum resistance thermometer
IR	Infrared
LDO	Low-dropout regulator
LED	Light-emitting diode
LSB	Least significant bit
MCU	Microcontroller unit
NPLC	Number of power line cycles
NTC	Negative thermal coefficient
PCB	Printed circuit board
PGA	Programmable gain array
PPG	Photoplethysmography
PSRR	Power supply rejection ratio
PTC	Positive thermal coefficient
RTD	Resistance temperature detector
SAR	Successive-approximation register
SHE	Self-heating effect
SMBus	System management bus
SPI	Serial peripheral interface
SPRT	Standard platinum resistance thermometer
SPS	Samples per second

Table of contents

List of figures

List of tables

1 Introduction

This master's thesis studies the practical accuracy of temperature sensors suitable for use in a wearable device. This chapter presents the background of the thesis, defines the goals and limitations for the study, and presents the overall structure of the thesis.

1.1 Background

The foundations for this thesis were laid out in the summer of 2018 when I was part of a research team in charge of developing a portable data logger suitable for a new way of energy expenditure (EE) estimation by augmenting traditional heart rate measurement data with the transferred heat energy from the person to the environment. This transfer of energy, or heat flux (HF), can be measured by using a HF sensor. Modern smartwatches supply multiple biosignal measurements for the user to see, however the heart rate based EE estimation has a typical error of 25 to 50 %. The EE error is most dominant during low intensity activities which are major part of normal day to day life which could be improved with the HF data of a person (Levikari et al., 2020). Typical hear rate sensors are based on photoplethysmography (PPG), where light-emitting diodes (LED) shine light into the persons body and a photodiodes measures the amount of light returned. As the heart pumps blood, the pressure inside the veins changes and so does the path which the light emitted by the LEDs has to travel to reach the photodiode. Pulsing the LEDs consume considerable amounts of power so they cannot be run continuously. For decreased power consumption such PPG sensor could be replaced by a high-resolution temperature sensor instead (Cuadras and Casas, 2006).

When HF measurements are conducted at least one temperature measurement is needed to convert the HF signal to the amount of energy transferred as HF is the flow rate of energy between two objects of different temperatures, the accuracy of this temperature measurement has a key role in the accuracy of the HF measurement. Considering how the HF sensor measures the temperature difference of two objects, equivalent results could be achieved using two or more temperature sensors

Figure 1.1. Subject from the project Q-Health wearing the first release prototype device equipped with HF and temperature sensors on his left hand. The device was used to measure EE from a wrist in a portable format with promising results when typical heart rate measurements were augmented with HF data (Levikari et al., 2020, Fig. 1.).

of high accuracy and resolution. HF sensors are typically more expensive than temperature sensors due to their uncommon nature, while temperature measurements are commonly used and manufactured in bulk volumes. In wearable applications the key factors for temperature measurements are accuracy, repeatability, resolution, and power consumption (Sapozhnikov et al., 2020).

1.1.1 Previous prototype

During the first prototype phase a wearable data acquisition system (DAS) in figure 1.2 was designed and built that included multiple sensors, for both environment and user measurements: skin and ambient temperature, ambient humidity, optical heart rate measurement to be supplemented by the HF data, a contactless thermopile for temperature measurement and multiple HF sensors to be attached to the subjects skin. Some of these choices have propagated through all the later prototype phases and are still prominent in this thesis, namely the analogue-to-digital converter (ADC) AD7124 capable of measuring the small signals generated by a HF sensor, the high accuracy LMT70 temperature sensor and a joint humidity and temperature sensor HDC2080.

The DAS was built on top of a RuuviTag and Nordic Semiconductor nRF52832

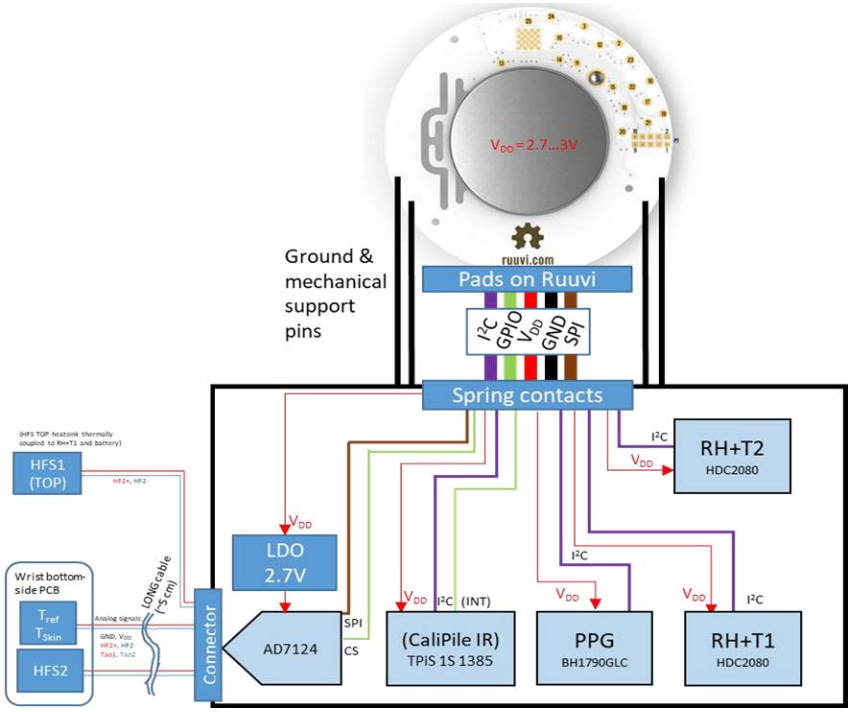

Figure 1.2. Diagram of the first wearable prototype device with on-board temperature and humidity sensors, optical heart rate, contact and contactless thermopiles (Kuisma et al., 2019, Kuva 11).

processor by using an external main board for the custom circuitry and another external sensor board that was attached to the subject.

1.2 Objective and limitations

In this thesis temperature sensors suitable for small biosignal measurements are studied and a test setup for few selected sensors is designed to conduct initial evaluation on their practical performance. Case requirements for the sensor performance are constructed based on the characteristics of the signals being measured by the client.

Sensor review will be conducted from readily available commercial sensors that can be integrated easily into the DAS under development by interfacing with either the available communications buses or by being compatible with the selected ADC. Multiple sensors with similar performance parameters can be selected for further evaluation to achieve broader overview into the available options. All the selections are made with wearables in mind and all the limitations that come with it, namely size and power consumption, however the designed test setup does not try to mimic

a wearable device form factor or power supply limitations. Designed ADC board should be able to be repurposed for other measurements than what are presented in this thesis.

Besides the measurement performance of the sensors, measurement repeatability is a point of interest when comparing the sensors. Emphasis is also placed on multisensory measurements for both analogue and digital sensors. Performance of the ADC in low power use cases is studied and a summary of the key features of the ADC is created to guide and aid the proper use of the device in future applications.

In tandem with this thesis a DAS development is conducted and as this thesis is to supplement the ongoing design process and further development of the DAS, certain limitations are placed for the sensor selection process that are discussed later in the thesis. The test setup and all measurements are documented in detail, due to time constrains the actual DAS integration is not discussed in this thesis.

1.3 Structure of the thesis

This thesis is composed of two major parts, the first three chapters are the theoretical part of this thesis studying practical temperature measurements in general, different sensor technologies available for use and the chosen ADC and chapters four to six present the design process of the physical test setup and completed measurements. The seventh chapter concludes the findings of this thesis.

First chapter provides the background and motivation along with the objectives and limitations for this thesis. In the second chapter a comprehensive literature review is conducted within the scope of this thesis on temperature measurements, different sensor technologies are studied and general considerations for sensor selection and use are presented. Sensors that are chosen for further evaluation are presented in detail and the final choices for the test setup are made. The third chapter presents a feature review of the selected ADC summarizing the key features and aspects that should be noted when using the device, some of which have been proven to be troublesome in the past prototype devices. Propositions for possible operating parameters are given regarding power usage and conversion performance.

Chapter four describes the requirements and the design process of the physical test setup. Planned measurements are presented and the configuration parameters for all chosen sensors are proposed. Chapter five presents the design process for printed circuit boards (PCB) capable of conducting all the required measurements.

Chapters six and seven present and analyse the results of the test setup and any observations that are made during the measurement process and provide a conclusion for the work of this thesis.

2 Temperature sensors

A literature review was conducted to gain more profound understanding of the various aspects of temperature measurements and how to select a temperature sensor suitable for accurate measurements. General considerations from the design point of view are studied and design questions related to the data logger prototype are explored and answered.

The following section studies the different temperature sensor types and their suitability for this particular use case. This study is the basis for the following sensor selection where the advantages and disadvantages of each sensor type are taken into consideration and combined with the use case requirements, five sensors are chosen for further inspection, and they are presented in table 1. Power consumption values are presented in appendix 2.

Table 1. Specification overview of the selected sensors.

Name	Type	Interface	Accuracy Typ Max [°C]	Resolution	Conversion time [µs]
TMP117	Thermal BJT	I^2C	±0.05 ±0.1	7.8 m°C	15.5
HDC2080	RTD	I^2C	±0.2	7.6 m°C	610
TMP006	Thermopile	I^2C	±1 ±3	>20 m°C	0.25
LMT70	Thermal BJT	ADC	±0.05 ±0.18	ADC	ADC
PT1000	RTD	ADC	±0.1+.0017*T ± 0.1765	ADC	ADC

2.1 Case requirements for temperature measurements

Based on previous knowledge of the type and magnitude of the biosignals to be measured, following requirements were set by the client to aid the sensor selection process presented in table 2. It was acknowledged that these requirements might not be completely achievable and resolution and suitable measurement range should be

prioritized over accuracy. As the focus of the wearable is portable human measurements, some durability aspects are considered ruling out bare sensor elements and otherwise delicate sensors as well as sensors that are too expensive for commercial consumer device.

Table 2. Case requirements for the temperature sensors, accuracy requirement should be met across the whole measurement range.

Accuracy [±°C]	Resolution [°C]	Operation range [°C]	Measurement cycle [Hz]
0.1	0.001	10-45	0.1

The DAS provides the interface for analogue sensors with the use of an ADC, for the use of digital sensors available communications buses are inter-integrated circuit (I^2C) and serial peripheral interface (SPI) which must be taken into consideration when selecting sensors. As the system is powered by a battery, power usage must be considered (Rahikainen, 2021).

2.2 General considerations for sensor selection

Design considerations are studied in this chapter regarding the physical implementation of the measurement system. Regardless of the used sensors, the heat must be transferred to the sensor element to accurately measure it. The methods of heat transfer are investigated and a suitable measurement topology for solid surface measurements is introduced.

Since the wearable is a portable battery operated device, the different power consumption aspects of the measurement system are investigated and suggestions for power conservation are presented. Multichannel measurements are explored, and the advantages and disadvantages of analogue and digital sensors are studied when the number of sensors is greater than what would be typically used, for example when array of temperature sensors is used to see temperature variations along a surface.

2.2.1 Heat transfer

Temperature measurement methods can be categorized as invasive, semi-invasive and non-invasive based on the interactions between the measuring sensor and the medium of interest. Invasive methods rely on placing the sensor in contact with the medium of interest and while doing so disturbing the thermal balance by transferring energy between the medium and the sensor. This heat can be transferred by the means of conduction when the medium is a solid or stationary fluid or through convection when the medium is gas or moving liquid. The flow of energy between two objects is called heat flux and in a solid one-dimensional objects it can be give by

$$q = -kA\frac{\Delta T}{\Delta x} \tag{1}$$

where q = heat flux, k = thermal conductivity, A = surface area, T = temperature and x distance (Childs et al., 2000). The transfer of heat can be promoted from a design perspective by increasing the surface area of the objects touching or by decreasing the distance the heat must travel through. For two or more bodies that are touching the heat flux is related to the thermal conductivity and the thermal contact resistance between the two bodies. This conductivity can be generally reduced by leaving air between two solid surfaces and it can be increased with the help of various thermal compounds replacing the air in between the two objects. For accurate modelling of heat transfer, the objects would need to be observed in three dimensions.

Exposed sensors, parts of the PCB and the medium of interest are subjected to heat transfer via convection. While the heat transfer coefficient is much lower than for conduction, 2.5-25 $\frac{\mathrm{W}}{\mathrm{m^2K}}$ for free convection versus 400 $\frac{\mathrm{W}}{\mathrm{m^2K}}$ for copper, it is still a significant source of heat flux when the temperature difference between the object and the surrounding fluid is increased. For convection heat flux is given by

$$q = h(T_s - T_f) \tag{2}$$

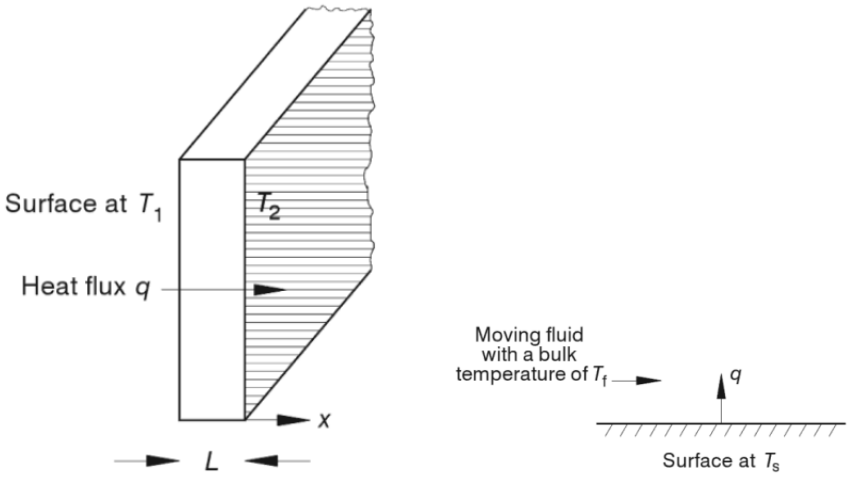

(a) Conduction through a solid or stationary fluid..

(b) Convection from a surface to a moving liquid or gas.

Figure 2.1. Heat transfer through the means of conduction and convection (Childs, 2001, Figures 2.2 and 2.3).

where h = the heat transfer coefficient, T_s = surface temperature and T_f = bulk fluid temperature. Generally convection is unwanted effect as it changes the ambient temperature on top of the sensors creating variations in measurements. Best way of avoiding the effects of convection is to cover the sensors from ambient temperature movements or by minimizing the contact area between the airflow by placing the PCB horizontally with respect to the direction of the flow.

Depending on the requirements for the temperature measurement, physical contact with the medium of interest could be undesirable or impossible to implement and in these cases non-invasive methods could be beneficial. Most non-invasive techniques are based on the electromagnetic spectrum of the medium of interest and majority of the visible light spectrum techniques are used for gases only. For solid objects infrared (IR) thermography is used since all matter emits thermal radiation when the object temperature is above 0 K.

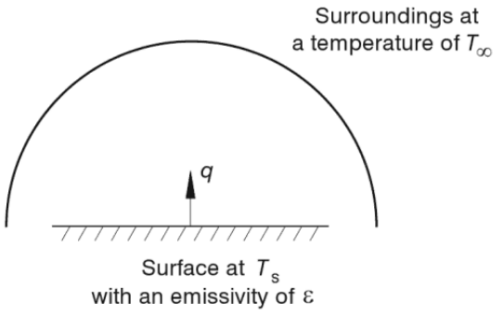

Figure 2.2. Heat transfer by radiation (Childs, 2001, Fig. 2.4).

Non-invasive methods have insignificant effect on the thermal balance of the medium of interest as they rely on observing properties emitted by the medium itself. Heat flux for radiant objects can be given by

$$q = \epsilon\sigma(T_s^4 - T_\infty^4) \tag{3}$$

where q = heat flux, ϵ = total surface emissivity, σ = Stefan-Boltzmann constant, T_s = surface temperature and T_∞ = Environment temperature. From equation 3 can be seen that by increasing the surface emissivity, for example by painting the measured surface with a blackbody-like material, the heat flux can be increased drastically.

Semi-invasive methods rely on temperature sensitive substances applied to the object to determine the temperature visually, usually by colour change. These methods can be non-reversible, and they provide only rough estimated of the object temperature. Disturbance to the temperature field is small. (Childs et al., 2000)

When a temperature sensor is physically interacting with the object to be measured, whether solid liquid or gas, there will always be heat transferred between two objects of different temperatures. Since the working principle of invasive thermal sensors is the measurement of physical temperature related changes within the sensor itself, this heat transfer is desired and the speed at which the temperature sensor physically reacts to the temperature changes of the measured object directly affects how responsive results can be acquired from the sensor. Therefore thermal mass of the sensor should be low and the thermal path from the object to the sensor should be of low resistance to ensure rapid reaction to temperature changes without disturbing the energy balance of the measured object.

When the temperature sensor can not be directly attached to the object being measured, for example due to being directly attached to a PCB, alternative methods of heat transfer must be considered. Typical integrated circuits (IC) are packaged within a moulded epoxy resin with small cross section making attachment of the sensor directly to the object difficult. Alternatively the PCB itself can be attached to the object with ease if the surface is solid, and level and the heat is transferred

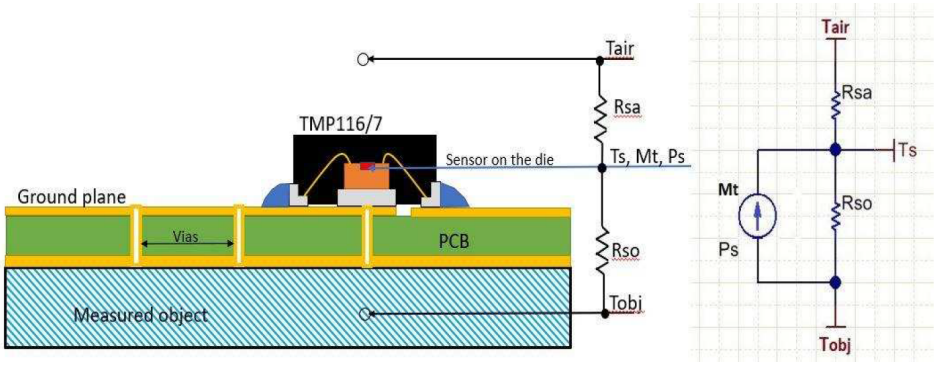

Figure 2.3. Temperature flow through PCB when measuring the temperature of a solid surface (TMP117, 2019, Fig. 1).

to the sensor via the ground planes and vias and through the solder joints of the device as demonstrated in figure 2.3. The thermal path consists of 3 different temperature sources regardless of what kind of topology is used, these are T_{obj}, T_{s} and T_{air} which are the temperature of the measured object, sensor inside the die and ambient air temperature surrounding the sensor. There will be thermal resistance between the sensor and object R_{so} and sensor and air R_{sa} regardless of if the sensor is directly attached to the object or covered by some insulating material acting as increased thermal resistance between the sensor and the ambient air. Average power dissipated by the sensor P_{s} will heat up the sensor from the inside and while doing so also locally heat up the surround area of the sensor. While typically low, this internal heating can build up within the sensor affecting drastically the measurement results. Lastly the thermal mass of the sensor and surrounding PCB area M_{t} influence the response time of the device, high thermal mass combined with high thermal resistance between the sensor and the object can lead to significant filtering of fast acting changes in temperature. Similarly any other heat generating components in the close vicinity will affect the measurement, most commonly these are other sensors or communication bus related pull-up resistors.

2.2.2 Power usage

For a wearable device that is run by a battery minimizing the power usage is critical. On the contrary, high accuracy measurements tend to have an increased power consumption even in a small form factor due to long measurement cycles leading to longer time spent in an active state. Since the required sampling interval is 0.1 Hz, we can conclude that the sensors will be spending majority of the time in some sort

of sleep or inactive state where the device typically has a low power usage regardless of the device. In an ideal situation the sensor package could be turned completely off, this will typically affect the start-up/settling time of the sensor negatively but due to the low sampling interval this shouldn't be a problem considering the power saving benefits it gives. When evaluating the power consumption of sensors, the microcontroller unit (MCU) is often overlooked as it is only used for interfacing with the sensor. Depending on the sensor type, reading data over the bus of complicated measurement sequences keeps the MCU in wake mode increasing the total power consumption of the measurement. Interrupt driven automatic measurement cycles should be favoured as these keep the MCU in deep sleep for most of the time decreasing power consumption drastically (Bui et al., 2019, Schackmann, 2019).

When multiple sensors and devices are run simultaneously prioritization of the shutdown states becomes important, as idling sensor current consumption can become a significant part of the total power consumed by the device. Dynamic power management should be employed where the device decides based on set parameters which devices need to be turned on at given time, as there are no real benefits from having all the sensors turned on if they can not be measured simultaneously (Simunic et al., 2000).

Power consumption estimation for data processing is difficult since determining when the MCU is working on the sensor data and when it is processing some other information not related to the current measurement is challenging, especially if the MCU is capable for interrupts, event prioritization or multitasking. If the selected sensor doesn't output temperature in a human readable format, which is the usual case with analogue sensors that output a voltage level, there are two options: the raw temperature related voltage value is saved directly to the measurement platform memory with the possibility of using excessive memory in return of lower power consumption, or the raw value must be processed into a temperature value by using additional MCU clock cycles. Depending on the mathematics required for converting the raw measurement value to temperature it might be beneficial to do some simple data manipulation on the raw value with the MCU to decrease the memory usage while avoiding demanding floating point operations if the available memory is low and measurement cycles are long. This type of data compression

is suitable for systems which doesn't display the received values to the user. When used in conjunction with data collection end point the raw or compressed values can be further refined into human readable temperature format on a device that is not reliant on the MCU on board power source.

2.2.3 Multichannel measurements

Multiple measurement channels bring its own challenges for both analogue and digital sensors. Number of digital sensors is limited by the used communications bus as the available unique device addresses are typically set by a combination of available pins being pulled high or low. In a typical I^2C sensor the amount of address pins is usually 2 at best, enabling a maximum of 4 unique device addresses. Some novel ways of circumventing this limitation exist: TMP117 has the capability of using the I^2C data and clock signals for the address pin, making it possible to have 4 unique addresses from a single address pin. When more sensors are needed, the devices can be split between multiple I^2C-buses which work in parallel. In principle two or more buses could share either a clock or data bus but this is not recommended, a more preferred way of multiplying the I^2C-bus is to have a MCU with a capability of multiple hardware or software I^2C-buses or to use a I^2C-bus multiplexer. I^2C being one of the few buses where the protocol device addressing is done by using software only, it can be expanded with relative ease (Bacciarelli et al., 2006, Leens, 2009).

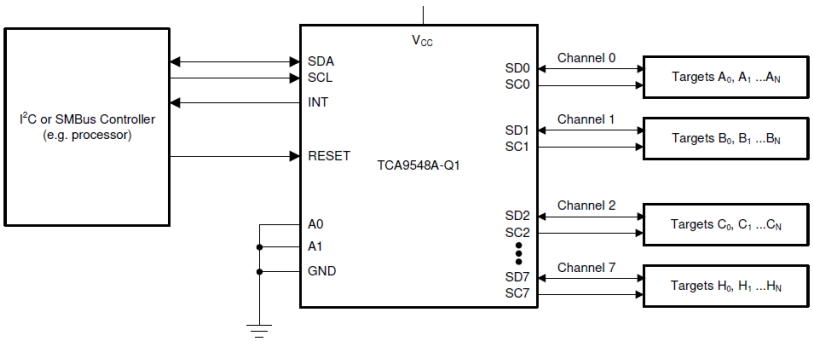

Figure 2.4. Simplified diagram of a I^2C-bus multiplexer. SDA and SCL holds the data and clock respectively, the same bus is used to control the multiplexer and to communicate with the target devices (TCA9548A, 2021, fig. 9-1).

Another popular communications bus is SPI, where instead of unique addresses each connected device is addressed by a general-purpose input/output-pin (GPIO)

dedicated for each sensor. With SPI the limiting factor is the available GPIO pins on the device, all data and clock pins are shared but each device requires a unique selection pin. This limitation can be solved by using a regular GPIO multiplexer or even a shift register. However the requirement for added hardware per device makes SPI more cumbersome to use when adding devices to the bus (Oudjida et al., 2010).

For analogue sensors typically the available ADC input channels is the limiting factor as normally only one measurement channel can be active at a time. This doesn't mean that only one sensor can occupy each input channel, only if the sensor has no way of being controlled externally it is the case. Another limiting factor is the fact that a single ADC has usually only one active input channel at a time, making simultaneous measurements impossible. The delay between two measurements can be configured by varying the conversion parameters, usually at the expense of noise-free resolution. When ADC output data rate is increased, the number of samples per conversion is reduced and the effects of unwanted noise increased. If the measurement circuit consists of several types of sensors that require multiple input channels, the change of channel between measurements influences the total output rate of the ADC due to the modulator and filter resetting and the ADC needing a full settling time to occur before next measurement can begin. There is typically also some dead time between the channel changes which can be noticeable especially with higher output data rates.

2.3 Sensor types

Most common sensor types were evaluated and their advantages and disadvantages compared, for commercial sensors price doesn't solely correlate with the accuracy of the sensor. When comparing different sensor following aspects were studied: accuracy, sensitivity, linearity, cost, response time and ease of use. Summary of the findings of this chapter are presented in table 3.

Only temperature sensors that output an electrical signal were evaluated due to the ease of use when combined with MCUs. For example sensors that use the temperature expansion of different materials exist, such as gas and liquid thermometers, but interfacing these with the chosen ADC or MCU can prove to be challenging and

was not seen as a practical approach for this thesis.

Table 3. Sensor technology advantages and disadvantages.

Type	Linear response	Advantages	Disadvantages
RTD	Yes	Stable Wide range Accuracy	Slow response Low sensitivity Price varies
Semiconductor	Yes	Low cost High sensitivity	Narrow range
Thermistor	No	Low cost High sensitivity Fast response	Nonlinear
Thermocouple	Depends	Low cost Rugged Wide range	Low sensitivity Accuracy
Thermopile	Yes	Non-invasive Fast reaction	Ambient T dependent Low accuracy Expensive

2.3.1 Resistance temperature detector

Sensor based on the fundamental property of every material, where the resistance of said material changes in relation to the temperature. For practical purposes not all materials make a great resistance temperature detector (RTD), most common materials include platinum, copper, silver and gold. Platinum RTDs are referred as standard platinum resistance thermometers (SPRTs) and they are used for the most demanding RTD applications where accuracy is key such as the definition of the international temperature scale of 1990 (Thomas, 1990). The sensor element is constructed by carefully wounding a thin wire onto a supporting structure to avoid any physical strain on the element. While this type of strain free SPRT has excellent measurement qualities, it is very prone to vibrations and shocks. For further protection from vibrations and physical shocks the element can be encapsulated by various materials, such devices are known as industrial platinum resistance thermometers (IPRT) and they are much more resistant to physical disturbances. (Childs et al., 2000).

RTDs are generally regarded as highly accurate and stable sensors with great re-

peatability, well suited for high precision applications across a wide temperature range. RTDs are passive by design so an excitation current is required to be able to observe the voltage drop over the RTD and to calculate the resistance of the sensor element. Regardless of the classification due to the resistance change being a physical property of the material, the resistance-temperature characteristics of a RTD is reasonably linear however to conform ITS-90 up to a 15th order polynomial is required when converting the resistance to temperature. Since voltage drop is observed there must be a power loss over the sensor which can be seen as internally generated heat, this is more commonly known as sensor self-heating effect (SHE) which can typically range between 0.2-3 mK in total depending on the excitation current and RTD resistance value (Batagelj et al., 2003). Some accuracy classes defined by IEC60751 are listed in table 4.

Table 4. Different accuracy classifications of RTDs, note how some classifications are derivatives of existing less accurate ones and they are valid for more narrow temperature ranges only (IEC60751, 2022). IST AG designations are presented, as the RTD used in this thesis is manufactured by them.

Class	± limit deviations in ° C (K)	IST AG designation
IEC60751 F 0.1	0.1 + 0.0017 * $\|t\|$	Y
IEC60751 F 0.15	0.15 + 0.002 * $\|t\|$	A
IEC60751 F 0.3	0.3 + 0.005 * $\|t\|$	B
IEC60751 F 0.6	0.6 + 0.005 * $\|t\|$	C
1/5 IEC60751 F 0.3	0.06 + 0.001 * $\|t\|$	K
1/10 IEC60751 F 0.3	0.03 + 0.0005 * $\|t\|$	K

2.3.2 Semiconductor temperature sensor

Semiconductors based on the p-n junction can function as a temperature sensor either by design or on accident, due to the forward bias voltage of the p-n junction being temperature dependent. As temperature increases, the bias voltage decreases linearly as illustrated in figure 2.5. Typically the maximum operating temperature is around 150 °C due to the junction reverse bias leakage current making the device unusable beyond that, but devices can be built to withstand up to 600 °C temperatures without affecting the linear temperature response of the junction voltage. However this temperature dependent property can introduce temperature related uncertainty to the circuit when the semiconductor device is not meant to be used as a temperature sensor, with proper design the changes in junction voltage can be used

for temperature sensing by using an external device like MCU or it can be used directly as a part of circuits with self correcting temperature behaviour (Vittoz and Olivier, 1979). Typically the characteristic voltage temperature relationship is ≈2 mV/°C for Si diodes and transistors giving us a rough estimated resolution of 2 μV/m°C (Hurley, 1958, McNamara, 1962).

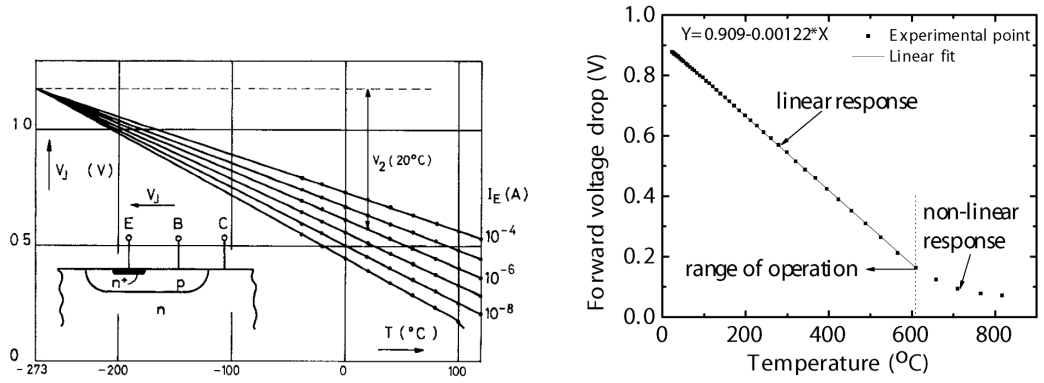

(a) Transistor base-emitter voltage (Vittoz and Olivier, 1979, Fig. 2.).

(b) Si diode forward voltage (Santra et al., 2010, Fig. 2.).

Figure 2.5. Linearity of the junction voltage change in semiconductors versus temperature.

2.3.3 Thermistor

Similarly to RTD discussed in chapter 2.3.1 thermistor is a device where the resistance of the component changes in relation to the temperature, however there are many differences between the two. Thermistors are typically manufactured from a semiconductor ceramic which can consists of multitude of materials. Thermistors can have either positive thermal coefficient (PTC) or negative thermal coefficient (NTC) which dictates the direction of resistance change compared to temperature. PTC thermistors increase in resistance when temperature rises, while NTC thermistors resistance lowers with the increase of temperature. Typically the R-T curve of a thermistor is exponential as shown in figure 2.6, in other words thermistors are much more sensitive at certain ranges for temperature changes than what RTDs are (Childs et al., 2000, Childs, 2001).

Typical thermistor accuracy is in the range of ± 0.1-1 °C as a cost saving measure of not needing to calibrate every sensor, but with the proper calibration techniques accuracy of ± 0.01-0.05 °C is obtainable with increased manufacturing costs (Childs et al., 2000). Due to the small size and therefore thermal mass thermistor have very

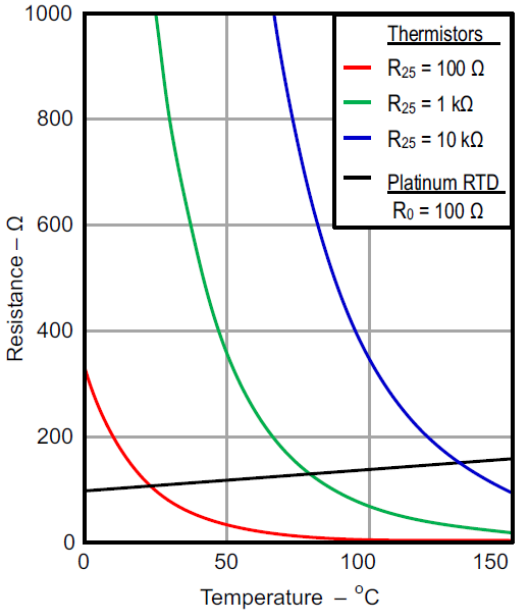

Figure 2.6. Comparison of R-T curve between three NTC thermistors and a RTD (Kuglestadt, 2019, Fig.3).

rapid response to temperature changes making them ideal for small bio-signals in human measurements or temperature monitoring for control systems. Due to more robust structure, thermistors are also more durable than RTDs being able to withstand mechanical and thermal shocks. The non-linearity and difficulties in finding accurate enough sensors were not in favour of thermistor in the selection process.

Being a resistive temperature sensing device thermistor requires a known excitation current which in turn leads to sensor SHE which can typically range between 0.2-3 mK in total depending on the excitation current and thermistor resistance value. Especially small tolerance thermistors are susceptible to decalibration and thermal related drift because of heat on the semiconductor materials as the materials age. Typically this aging drift increases the resistance of the element over time as exposure time to temperature changes increase. In room temperature thermistors are typically stable (Wood et al., 1978, TE, 2018).

2.3.4 Thermocouple

Thermocouple is formed when two metals with different thermoelectric powers are attached to each other and when the whole constructed device experiences a thermal gradient a voltage is generated along the length of the thermocouple. The thermal

electromotive force (EMF) across two points of different conducting materials is called Seebeck effect, in an open-circuit the gradient voltage is proportional to the gradient temperature, technically any two conducting materials could form a thermocouple but in practice there are some combinations that are better than others. Unintentional thermocouples can be formed between connection points across the circuitry generating parasitic thermo-EMF that can be of several micro volts in magnitude (Immonen, 2019).

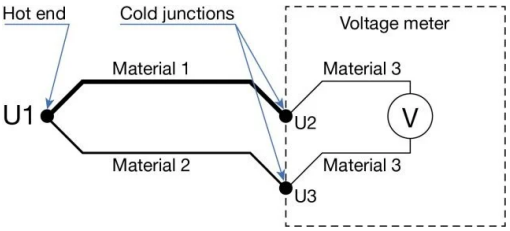

Figure 2.7. Cold junction with no compensation causes thermovoltages U2 and U3 to be connected in series with the wanted measurement U1 spoiling the measurement result (Laurila, 2017, Graph 4).

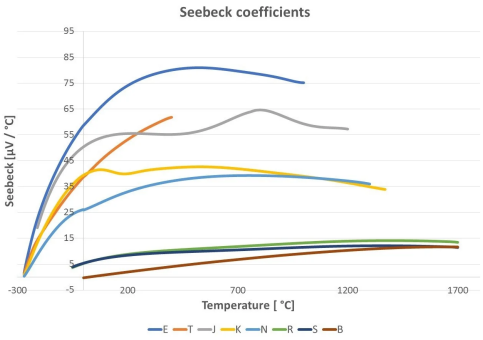

Figure 2.8. Seebeck coefficient determines the sensitivity to temperature changes of the formed thermocouple; some thermopiles have linear Seebeck coefficient while for others it can be a bit sporadic (Laurila, 2017, Graph 3).

The Seebeck coefficient which determines the sensitivity of the thermocouple can be of varying shapes shown in figure 2.8. For some thermocouples, like types B, S, and R, the coefficient is linear across the whole measurement range. Benefits of thermocouples include very wide temperature range of -270-3000 °C suitable for many industrial applications, relatively low cost and robustness of the sensing element, while the typical measurement accuracy of ± 1.5 °C is a disadvantage (Childs et al., 2000). For human measurements the excessive temperature range of thermocouples was seen unfit as it affected some other aspects of the sensor characteristics.

For thermocouple to work properly the so called cold junctions must be considered, various compensation methods are presented in figure 2.9. When handled improperly, additional thermovoltages are generated at the thermocouples formed by joining the sensor wires to the voltage meter or ADC connection points typically made from different material than the sensor element. There are three options that

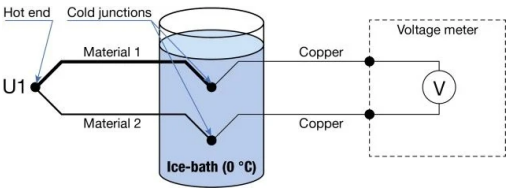

(a) 0 °C ice bath for stable known temperature, used for laboratories and calibration.

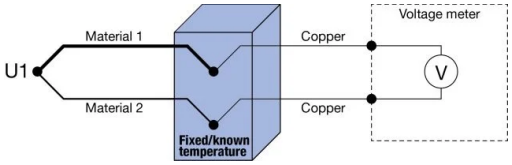

(b) Known temperature at the cold junction.

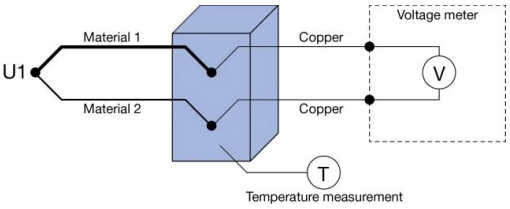

(c) Measured cold junction temperature.

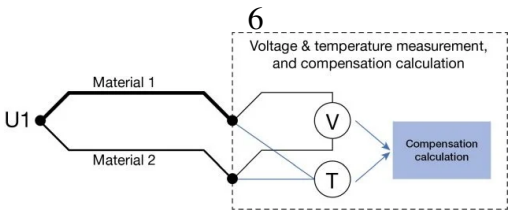

(d) Automated cold junction compensation, the device measures cold junction temperature and completes the compensation calculations.

Figure 2.9. Different cold-junction compensation methods, some are more practical than others (Laurila, 2017, Graphs 5-8).

can guarantee the cold end compensation to not spoil the measurement data. The cold junction can be placed in an ice bath at 0 °C, where the junction inherently generates no thermovoltages due to the temperature. While ice bath is the easiest solution in short term, it is not suitable for many industrial applications or continuous use due to condensation and the need of more ice as the existing ice melts away. Second possibility is to place the junction in a known temperature and keep the temperature stable, however this required accurate temperature control of the ambient temperature and the ability to monitor said temperature. Last possibility is to measure the temperature of the cold junction. In both known temperature cases an offset value can be calculated representing the cold junction thermovoltage and this can be subtracted from the actual sensor value. Any of the three methods is a practical option, although measuring the cold junction temperature is typically most practical case outside laboratory environment as it can be done with another temperature sensor and an ADC that is already required to measure the thermocouple (Laurila, 2017).

2.3.5 Thermopiles

When several thermocouples are connected in a certain way in series, or less commonly in parallel, a thermopile is formed. Alternating thermocouple pairs are arranged between the two sides of a thermopile, when a temperature difference is observed between the two sides of the sensor proportionally equal voltage is generated on the output. By extension this voltage is also proportional to the heat flux moving through the thermopile and thermopiles are used in heat flux sensors for monitoring the flow-rate of thermal energy between two objects. Due to the non-invasive nature of the measurement and the use of thermocouples, reaction to changes in temperature is fast (Goldsmid, 2016).

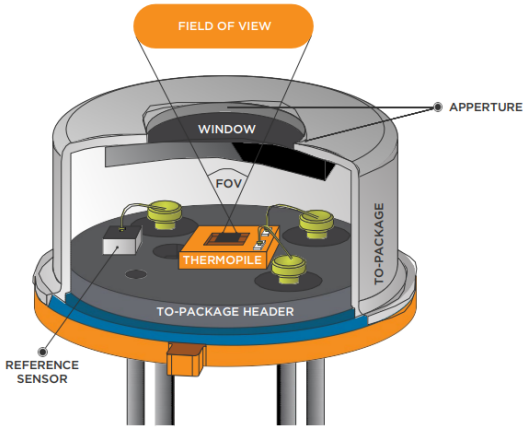

Figure 2.10. Cross section of a thermopile sensor, thermopile detects the IR radiation through the window which is typically made of IR filtering material. The reference sensor is needed for the cold side temperature (TE, 2021, Fig.1).

Most common use case for thermopiles is non-invasive temperature measurements, where the amount of IR radiation of the object of interest is measured and converted into temperature. When the IR radiation hits the thermopile sensor it gets absorbed by the sensor surface and converted into heat. Due to thermopiles not reacting to the absolute temperature, but the temperature difference between the two sides, a reference temperature of either side of the sensor is needed to correctly calculate the temperature being measured. Further few fundamental constraints must be known to get accurate temperature readings: The surface emissivity of the object and the placement of the sensor in relation to the measured object. As the sensor output voltage is proportional to the IR radiation that hits the sensor and every material emits different amounts of IR radiation when at certain temperature, sufficient IR radiation amount must reach the sensor for any accurate measurements. Ideally the

sensor measures a black-body radiation of an object with a surface emissivity value of 1, but in real world this is not the case. Surface emissivity value higher than 0.7 is typically suitable for measurements, however values above 0.9 are recommended. For reference the human skin has a surface emissivity value of 0.98 (Charlton et al., 2020, TMP006, 2011).

Measurement geometry and ambient air quality should be considered when conducting measurements, typically the sensor field of view can be wide and unwanted IR radiation can hit the sensor or humidity and small particles in the air can block some of the IR radiation spoiling the measurement results. For accurate measurements the sensor should always be calibrated for a certain system only (TMP006, 2011).

2.4 Digital sensors

Three digital sensors were chosen for further tests, the main criterion being accuracy, power consumption and ease of use. In these three categories TMP117 has the best accuracy of ± 0.1 °C, HDC2080 has best typical power consumption of 300 nA and TMP006 the ease of use from a mechanical standpoint for being a contactless sensor.

Benefits of digital sensors are easy to see when considering multichannel measurements. Unlike with analogue sensors where the limiting factor is the availability of simultaneous conversion channels, which is usually one, each digital sensor can complete measurements on its own and only require a shared communications bus to run. Limitations of various communications buses are discussed in chapter 2.2.3.

2.4.1 TMP117

High precision digital temperature sensor with accuracy of $\pm$ 0.1 °C or less as shown in figure 2.11 with a resolution of 7.8 m°C. Maximum quiescent current of 220 μA during active conversion, 0.5 μA when in shutdown mode. Sensor communicates through SMBus or I^2C bus and has an electronically erasable programmable read-only memory (EEPROM), which allows the user to program the sensor once

and it will reload wanted operating parameters from memory on subsequent restarts. This can be utilized in the synchronization of measurements of multiple sensors by issuing an I^2C general reset call, for which every device reacts and begins conversion according to the pre-programmed instructions. A maximum of 4 devices can share the same bus due to address limitations.

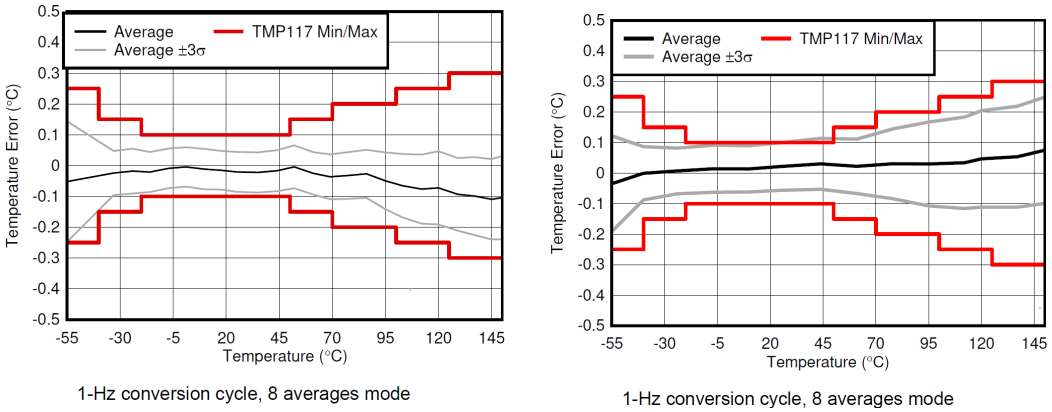

(a) DRV package. **(b)** YBG package.

Figure 2.11. Accuracy of TMP117 as a function of temperature for both available package types. Within the required temperature area, accuracy can be lower than ± 0.1 °C. (TMP117, 2021, Fig. 6-2 and 6-3) Temperature error can be further lowered with increased averaging modes.

For interrupt driven applications the device comes with a programmable alert pin, which can be used as an indicator for the MCU when conversion is ready to be read from the device. There is also a possibility of pre-programmed conversion standby time, during which the device sits in shutdown mode between subsequent measurements. This can enable autonomous measurements without any additional effort from the processor besides reading the conversion result on interrupt. Available delays range from 15.5 ms to 16 s, with 8s being closest to the wanted 0.1 Hz sampling interval.

If the application has multiple TMP117 sensors doing simultaneous measurements, the MCU should wait until all sensors have finished with the conversion results before collecting the measurement data to avoid causing any interference with the ongoing measurements.

Great care should be taken when soldering the component to a PCB, as the heating of each pad creates mechanical stress within the silicon die which can lead to unpredictable soldering shift of up to ± 100 m°C or up to ± 150 m°C when hand soldering. This soldering shift can be reduced by leaving the thermal pad of the

sensor unsoldered as seen in figure 2.12 noting that leaving the thermal pad unsoldered will roughly double the thermal resistance between the sensor and PCB and that way will increase the thermal response time of the device.

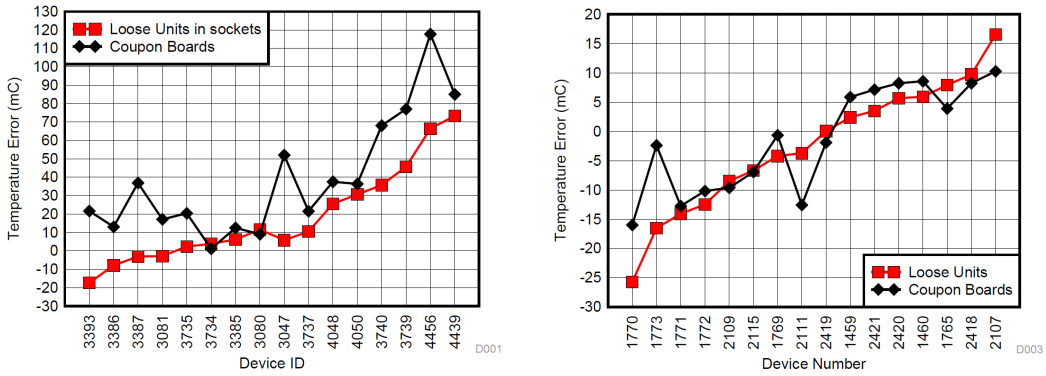

(a) Thermal pad soldered to PCB. **(b)** Thermal pad not soldered to PCB.

Figure 2.12. Soldering shift at +25 °C, 3.3 V. Leaving the thermal pad unsoldered can significantly reduce the unpredictability of the temperature error of the sensor. (TMP117, 2019, Fig. 6 and 7).

Device SHE should be considered if conversions are made continuously, depending on the supply voltage the device can dissipate up to 1 mW of power. In this application where measurements are taken roughly 10 seconds apart and the device spends most of the time in standby mode between measurements, SHE is lower as the sensor has time to dissipate any accumulated heat during the shutdown phase (TMP117, 2021).

2.4.2 HDC2080

Low power temperature and humidity sensor with a temperature accuracy of $\pm$ 0.15 - 0.2 °C as seen in figure 2.13, 8 m°C resolution, and a very low power consumption of average of 0.105 µA at 1 measurement every 10 seconds. Suitable for battery operated portable applications due to its low power usage in comparison to other sensors, however only 2 devices can share the same bus due to address limitations. As the sensor is a joint humidity and temperature sensor, there was little info available on the type of temperature sensor inside. Typically in humidity applications RTDs are used due to their stability and the ability of using the RTD as a heating element for accurate >90 % humidity measurements.

The sensor has a configurable auto measurement mode with sampling range of $\frac{1}{120}$

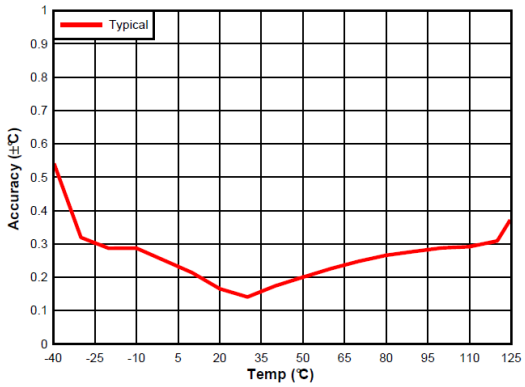

Figure 2.13. HDC2080 temperature accuracy versus measured temperature, which varies between 0.15 °C and 0.2 °C within our temperature range discussed in chapter 2.1. (HDC2080, 2021).

to 5 Hz and a configurable interrupt pin for independent operation from the MCU, which further reduces the total power consumption of the device as a part of a system. For multichannel measurements the device imposes a limitation of having the possibility of only two I^2C addresses available which limits the number of devices per I^2C-bus.

2.4.3 TMP006

Low power digital thermopile sensor with a typical accuracy of $\pm$ 1 °C, and a supply current of 240 µA when active. Due to the nature of thermopiles an ambient temperature sensor is needed for contactless temperature measurements, thermopile has a resolution of 22 m°C and the local temperature sensor resolution of 0.031°C (TMP006, 2012).

When conducting measurements with this sensor a few constrains need to be known for accurate results: the surface emissivity of the target object and the placement of the sensor relative to the target object. Measured object should be placed in a way that the IR radiation hits the sensor at a straight angle, as this is the most sensitive direction for measurements as seen in figure 2.14b. Other radiating bodies in the proximity of the measured object can interfere with the measurement considering the field of view of the sensor is wide and it can detect IR radiation even at high angles. By keeping the angle of incidence as close to zero as possible unwanted IR radiation can be avoided. Typically the object should be no further than half of the radius of the target away. Once the sensor is placed in a suitable position for mea-

surements, the sensor needs to be calibrated for the system. Calibration is essential for accurate measurements, as without the calibration factor the object emissivity and the field of view the object is occupying are not accounted for (TMP006, 2011).

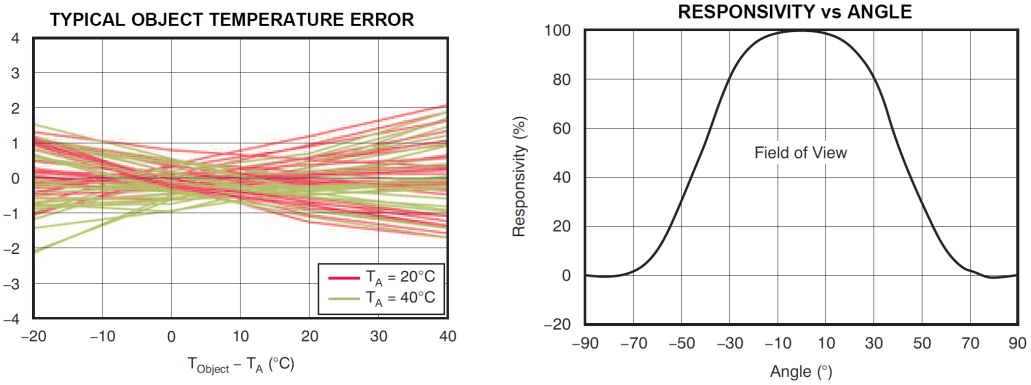

(a) Typical object temperature error with different ambient temperatures.

(b) Sensor responsivity to IR radiation versus angle.

Figure 2.14. Accuracy and sensitivity of the sensor (TMP006, 2012, Figures 1 and 3).

Instead of I^2C this sensor communicates using system management bus (SMBus), a communications bus compatible with I^2C. Main differences between the two are in trivial details that can be usually ignored for normal use. Pull-up resistor values and current running in the bus, logic voltage levels and signal rise and fall times. A novel way of using only two address pins and the data and clock lines as valid states enables eight sensors to be present on the same bus similarly to TMP117 (Maxim integrated, 2000, Schackmann, 2019).

2.5 Analogue sensors

Two distinct types of analogue sensors were chosen for further tests: a RTD PT1000 which also acts as a reference sensor and a semiconductor based LMT70. Analogue sensors typically give more flexibility in terms of the output signal, so each measurement design can be tailored for the input and gain range of the used ADC.

2.5.1 LMT70

Very linear CMOS analogue temperature sensor, with low power consumption and an approximate resolution of 5 µV/m°C. The sensor has an accuracy of ± 0.05 °C within the temperature range of 20-42 °C and ± 0.2 °C within the temperature range

of -20-90 °C as shown in figure 2.15b. Suitable for multichannel measurements due to an enable pin on each sensor module, which allows multiple LMT devices to share a single ADC channel. When combined with a shift register, a single GPIO-pin can cycle through all the sensors and reset the ADC between every change. Due to the low power consumption of max 12 µA, it can be powered via the AD7124 digital output pins that can source a maximum of 100 µA of current. Since the power usage the sensor is low, SHE is very low, and the sensor dissipates less than 36 µW. When sensor temperature matching is important, the A variant can be used as adjacent sensors on the tape and reel are temperature matched within 0.1 °C.

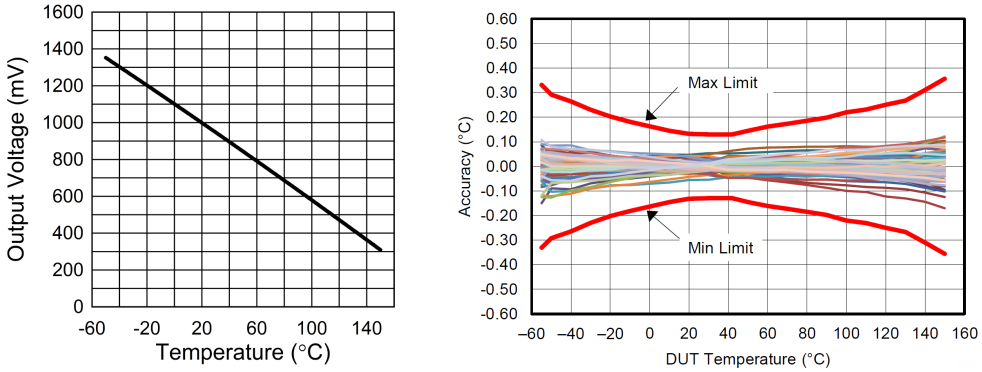

(a) Linearity of output. **(b)** Accuracy.

Figure 2.15. Output linearity and accuracy of LMT70 across temperature range (LMT70, 2015). Accuracy of output across over 10 °C ranges can be improved by using linear interpolation and look-up tables.

When aiming for maximum power savings the sensor can be turned completely off instead of using the T_{ON} pin, this in turn increases the output settling time from 30-500 µs to 0.6-1 ms. If measurement cycle is 0.1 Hz, the change in power-on time is negligible and the power usage drops from 12 µA to 50 nA.

Due to the semiconductor nature of the sensor, the temperature sensing element is extremely sensitive to light, especially IR, even when inside the sensor packaging. When employing the sensor, ambient light conditions should be considered and necessary precautions to be taken to limit the light exposure of the sensor package (LMT70, 2015).

2.5.2 PT1000

A Y-class PT1000 was chosen as a reference temperature sensor due to the stability, accuracy and low power consumption which equals to smaller SHE when running the sensor at 100 µA. With a temperature dependent accuracy of $\pm 0.1 + 0.0017 * |t|$ °C this sensor was the most accurate sensor available that was interfaceable with the used digital multimeters (DMM) in the test setup. Considering the aim of this thesis a PT1000 was more suitable than PT100 as the output signal will be ten times bigger in magnitude and the power consumption is ten times smaller resulting in smaller SHE making it more suitable for wearable applications.

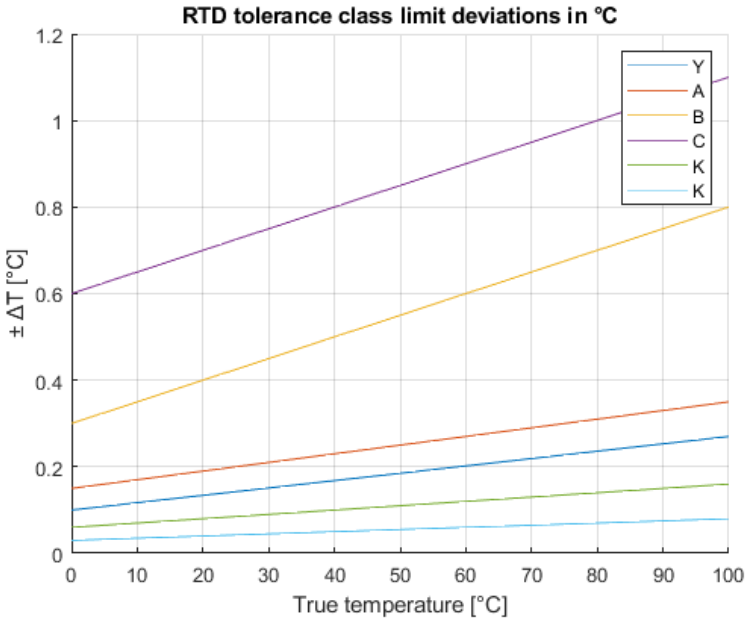

Figure 2.16. RTD limit deviations over the range of 0-100 °C range, for purposes of this thesis main focus will be in the range of 10-45 °C (IEC60751, 2022).

As the sensor can be interfaced with both the reference DMM and the used ADC, it can be used to evaluate the performance parameters of the ADC in a way that eliminates the differences originating from dissimilar sensors.

3 Analogue-to-Digital converter

Typically general use MCUs includes one or more embedded ADC channels to be used with user interface controls, simple analogue sensors or to check the device battery level for example. For such applications the embedded ADC is generally good enough in terms of accuracy, resolution, and conversion times that the conversion results are acceptable. For more precise measurements, such as the temperature measurements of this thesis, the embedded ADCs are lacking. For comparison the DAS embedded ADC is a 14-bit 8 channel successive-approximation register (SAR) ADC, compared to the external 24 bit $\Sigma - \Delta$ ADC used.

For the previous prototypes measuring HF an AD7124-4 $\Sigma - \Delta$ ADC was selected due to its low noise 24 bit inputs, low power usage, and versatile configurations available making it functional for variety of measurements. With eight input channels, programmable gain setting and the possibility for external excitation the ADC can function independently in varying measurement configurations. Figure 3.1 presents the block diagram of the ADC with the available I/O. The ADC can function in both 3-wire and 4-wire SPI modes with the possibility for interrupt driven operations and measurement sequencing making it independent device from the MCU once properly configured. Data integrity can be validated with checksum for precise communications.

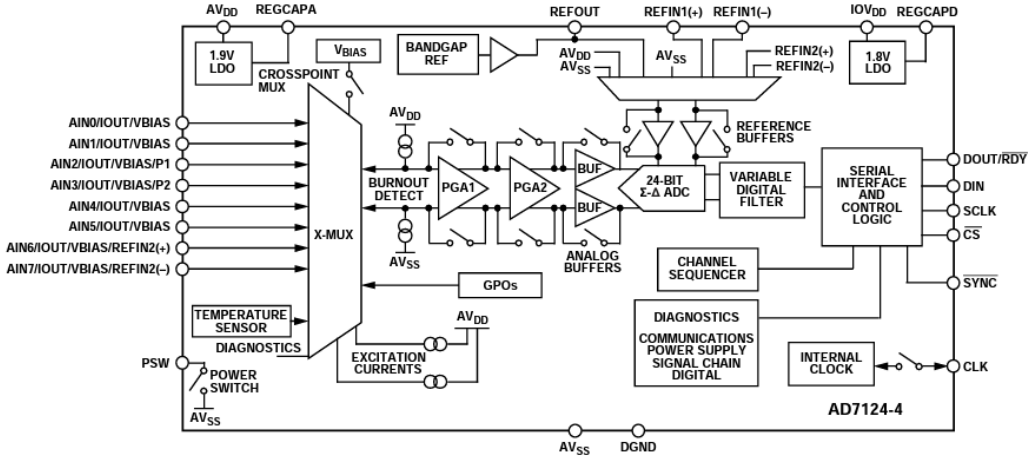

Figure 3.1. Functional block diagram for the ADC. It is worth noting how some of the functionalities share pins with other functions of the ADC which must be taken into consideration when designing the front end (AD7124, 2018, Figure 1.).

The type of the ADC imposes limitations on the resolution and data rate of the measurements, typically higher resolution means lower sampling rate as shown in

figure 3.2a. By design $\Sigma - \Delta$ ADC samples multiple times over a set time period which hinders the reaction to quick changes in the input signal but provides more noise free bits for the result. This is a desirable effect when conducting accurate measurements that are small in magnitude, but in turn the ADC filters out small variations in the signal. This filtering can affect noise which is desirable, but it can also filter out parts of the desired signal being measured. The typical high resolution of $\Sigma - \Delta$ ADC can allow direct measurements of small signal sensors without the need for any special front end considerations (Kester, 2008, 2005). For alternative ADC architectures such as SAR ADCs the signal sampling can be executed with the use of sample-and-hold circuitry to respond to rapidly changing signals with a stable sampling signal, these conversion results reflect more accurately the momentary status of the signal. For high speed applications pipelined ADC can be used, where the sampling required exceeds 1 MSPS when resolution can be spared. For the intended measurements the benefits of SAR and pipelined ADCs don't match with the requirements and therefore $\Sigma - \Delta$ ADC is the correct choice for this application (Kester, 2005, Baker, 2006)

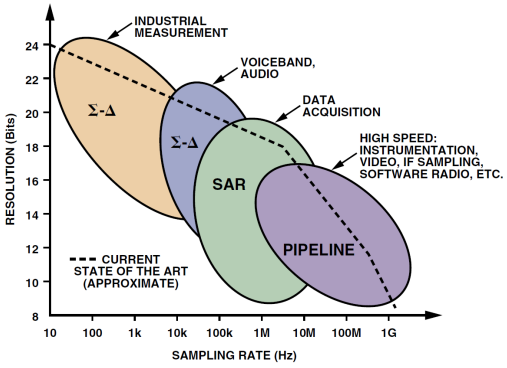

(a) Different ADC architectures and their suitability based on required resolution and sampling rate. (Kester, 2005, Figure 1.).

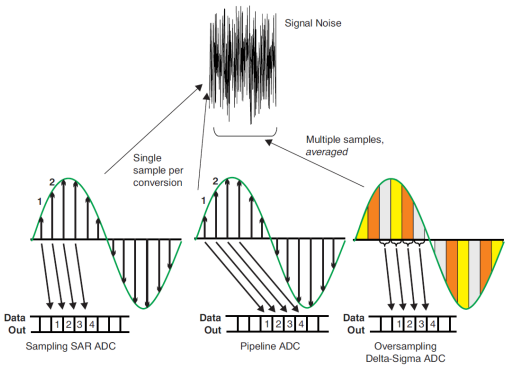

(b) Different sampling styles of the various ADC architectures (Baker, 2006, Fig. 1).

Figure 3.2. Comparison of different ADC architectures.

3.1 Control registers

Using the control registers ADC_CONTROL and IO_CONTROL_1 the user can configure parameters affecting every measurement. It is important to note that these settings can not be set to change automatically with measurement channels

but instead they reset the filter and modulator when written into in a similar way as pulsing the $\overline{\text{SYNC}}$ pin does, because of this the use of single conversion mode is recommended when manipulation of control registers is needed in between measurements. If used with the sequencer, care should be taken that all control register changes take place before the ongoing conversion is completed. In an interrupt driven system this can lead to incorrect control parameters being set for the next conversion if the timing is incorrect, especially if the data rate is high and the window for changes is narrow.

3.1.1 Power modes

There are 3 power modes available: full, mid and low power. The current consumption and available output data rate range are both dependent on the power mode, which also influences the effective noise free resolution of the ADC. Furthermore when designing the sensor circuitry the output signal level should be considered to avoid certain gain ranges, as the offset error drift of the ADC is not linear and is the greatest at gain levels between 2 to 16.

Table 5. Effects of ADC power modes on performance parameters (AD7124, 2018, Table 3.). In some low power applications the small increase in current draw for mid power mode can be beneficial.

	RMS noise [nV]	Output data rate [SPS]		p-p resolution [bits]	Current draw [μA]	Temperature offset error [nV/° C]		
		Min	Max			Gain 1 or >16	2 to 8	16
Low	24	1.17	2400	16.4	255	10	80	40
Mid	20	2.34	4800	17.1	355	10	40	20
Full	23	9.38	19200	18	930	10	10	10

For further power savings the ADC can be set in power-down mode which limits the power consumption of the device with the expense of longer start-up time and having to re-configure the ADC as all the internal registers have reset to their default values. With calibration coefficients saved into the MCU and when used with low rate of measurements, power-down mode instead of standby can reduce the power usage of the device by 80% when not taking into account the MCU power usage of re-configuring the ADC.

Table 6. Power supply currents for both analogue and digital sides while in standby and power-down mode. Idle mode is also available, but it is mainly used with the calibration steps of the device (AD7124, 2018, Table 3.).

	$I_{\mathrm{AV_{DD}}}$ [µA]		$I_{\mathrm{IO_{VDD}}}$ [µA]	
	Typ	Max	Typ	Max
Standby	7	15	8	20
Power-down	1	3	1	2

3.1.2 Conversion modes

Three conversion modes are available for the user to choose: Single conversion, continuous conversion and continuous read. In single conversion mode the user activates the conversion and the ADC sequences through all enabled channels completing each conversion and beginning the next one. Previous conversion result must be retrieved within a limited time window before the next conversion finishes, or the result will be lost. Once all enabled channels are completed, the ADC returns to standby mode. Conversion readiness can be either read from the appropriate status register or read from the $\overline{\mathrm{RDY}}$ pin directly.

In continuous conversion mode the ADC sequences through all enabled channels and begins the loop from the beginning. Once the measurement has started, the device operates on its own. If completed conversions are not read in time, they are cleared and replaced with new conversion results. This is also the default mode in which the ADC begins its operation.

In both single and continuous conversion mode the completed conversion result can be re-read from the device as many times as the user wishes, and it will only be replaced by a new result if one has completed. However in continuous read mode the conversion result can be read only once. Continuous read mode is an extension of continuous conversion mode, enabled by setting the CONT_READ bit in ADC_CONTROL register. Once enabled the only way to see if conversion is ready is from the $\overline{\mathrm{RDY}}$ pin as sending a read command when there is no conversion result ready will move the device back to continuous conversion mode.

For multiple enabled channels it is good practice to enable the DATA_STATUS bit in ADC_CONTROL register, so on every data read the contents of the status register

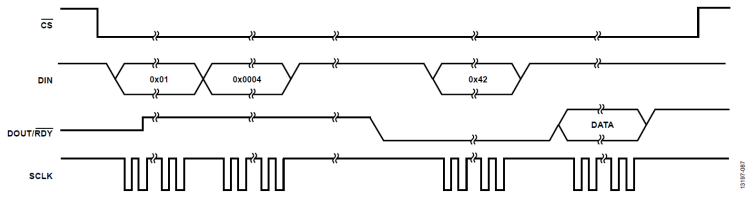

(a) Single conversion mode. DIN: write - command - read.

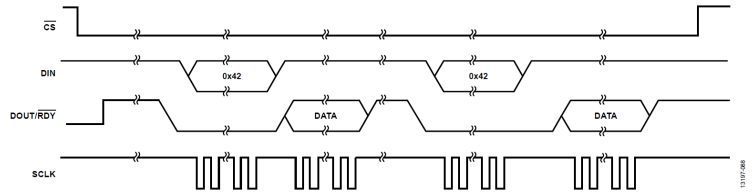

(b) Continuous conversion mode. DIN: read - read.

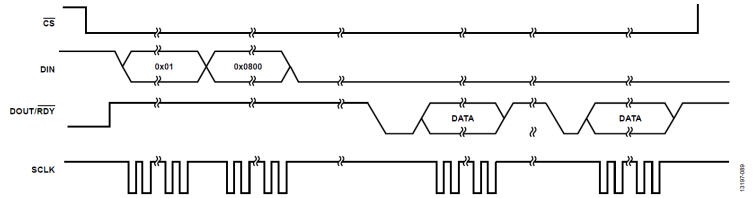

(c) Continuous read mode. DIN: write - command - data available at DOUT without further instructions.

Figure 3.3. Different conversion modes and how they affect the SPI communication between ADC and MCU per measurement cycle. When $\overline{\mathrm{CS}}$ is pulled low, completed conversion is indicated by $\overline{\mathrm{RDY}}$ going low (AD7124, 2018, Figures. 82-84).

are also sent along the conversion result. The status register contains any possible error flags that have been triggered during the conversion process, also the current measurement channel number is included for easy identification of the received measurement result.

Each conversion mode has its own benefits and drawbacks. Since IO_CONTROL_1 register should not be controlled while performing active conversions, due to the conversion circuit changes while active conversion is on the way, changes to the digital logic pins P1 and P2 and the excitation current need to be coupled with a pulsed $\overline{\mathrm{SYNC}}$ pin. After changes to the circuit have been made, a falling edge signal to the $\overline{\mathrm{SYNC}}$ pin will reset the active filter and modulator back to an initial stage without changing any of the existing register settings or the position in sequencer queue. The filter and modulator are held in this reset state until the $\overline{\mathrm{SYNC}}$ pin receives a rising edge signal, and the conversion begins from a stable circuit state. Modulator and filters can be also reset by writing into the mode or configuration register.

3.1.3 Input/Output

The ADC contains two configurable constant current sources that can be individually set to source current between 0-1000 µA with fixed steps to any of the AINx analogue input pins. Only one analogue input pin can be selected per current source, but the two current sources can output to the same analogue input pin. The two current sources are current matched to $\pm$ 0.5 % when V_{out} = 0 V, suitable for ratiometric measurements.

Two logic outputs, P1 and P2, are user controllable through the IO_CONTROL_1 register and they are located at input pins AIN2 and AIN3. The pins function as regular input channels until enabled by the GPIO_CTRL# bits when they can be individually set to logic 0 or 1. These pins can be used to control the status of external sensors or logic controlled multiplexers. Changes to these pins while conversions are active should be coupled with pulsing of the $\overline{\mathrm{SYNC}}$ pin detailed in chapter 3.1.2 if the logic changes change the current measurement circuit.

A togglable low-side power switch is located on the PSW pin and it can be controlled with the PDSW bit. The switch is connected to the $\mathrm{AV_{SS}}$ and can sink a maximum of 30 mA of continuous current. It can be used to toggle on and off measurement circuits that are interfaced with the ADC when not in use for power saving purposes.

3.2 Channel and configuration register

There are total of 16 pre-programmable measurement channels located at registers CHANNEL_0-15, each which can have any combination of the available input channels as the positive and negative input. Besides the analogue input channels possible inputs are the internal temperature sensor, $\mathrm{AV_{SS}}$ and DGND, the internal 2.5 V reference and diagnostics inputs used to monitor the state of the power supply voltages, regulator voltages or to apply an internal test signal to the channel. Each channel register can be assigned one of the 8 available setups numbered 0-7 with the Setup bits, a single setup includes a corresponding configuration, filter, gain and offset register. Multiple channels can share the same setup if required as illustrated

in figure 3.4. For every measurement cycle the sequencer will cycle through all the channel registers with their enable bit set to 1, the measurement order is always from the lowest number to the highest and this can't be changed.

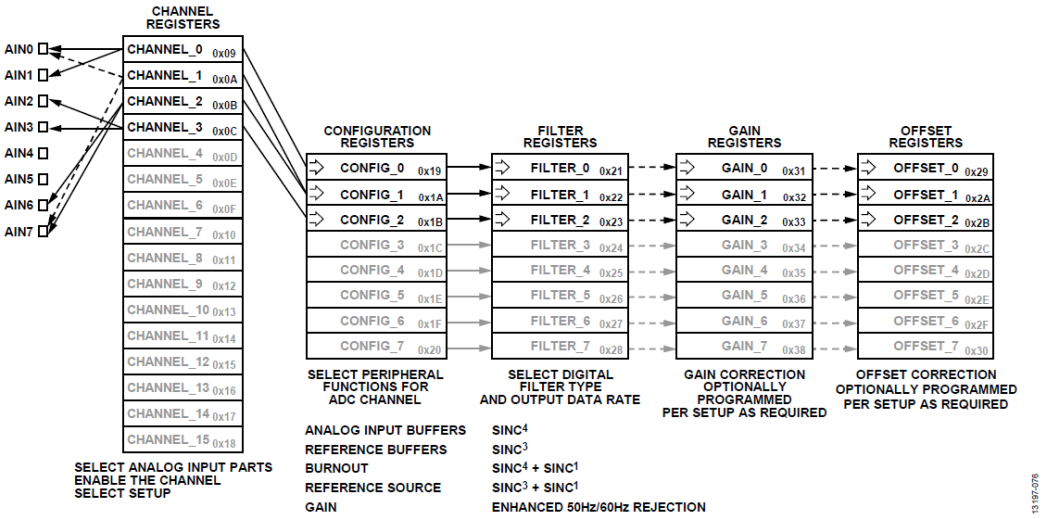

Figure 3.4. Illustration of the flexibility of channels and configurations. Channels 0-3 are enabled and are used by the sequencer; each channel has a unique combination of analogue inputs. Channels 1 and 2 share a setup consisting of configuration, filter, gain and offset registers. (AD7124, 2018, Figure 73.).

Shared setup between different channel registers is useful when there are multiple identical sensors to be measured, this way every sensor is measured using the same settings from configuration, filter, gain and offset registers to minimize any ADC related errors. However at some sensor configurations where the signal paths differ between similar sensors, separate calibration might be required via different setups.

3.2.1 Programmable gain array

Programmable gain array (PGA) bits can be found from the configuration register and they change the gain of the two internal amplifiers to utilize the whole 24 bit measuring range of the ADC, increasing gain lowers the max voltage that can be measured. When choosing sensors and designing the possible pre-amplifier stage it should be noted that in low and mid power modes the gain range of 2 to 16 suffers worse offset temperature drift than gain stages of 1 or >16 as shown in table 5. For a worst case scenario of 35 °C temperature difference and 80 $\frac{\text{nV}}{\text{°C}}$ the temperature drift could produce up to 3 µV of offset in the measurement. When using gain 1, the positive and negative input can be unbuffered or buffered at the users will,

Table 7. ADC input range and resolution with different PGA settings and V_{ref} voltages. When operating in unipolar mode only positive voltages are accepted and the resolution is halved.

Gain	Input range (Bipolar Mode) and resolution per bit					
	V_{ref} = 2.5 V		V_{ref} = 0.5 V		V_{ref} = 0.6 V	
	[mV]	[nV]	[mV]	[nV]	[mV]	[nV]
1	±2500	298	± 500	59.6	± 600	71.5
2	± 1250	149	± 250	29.8	± 300	35.8
4	± 625	74.5	± 125	14.9	± 150	17.9
8	± 312.5	37.3	± 62.5	7.45	± 75	8.94
16	± 156.25	18.6	± 31.25	3.73	± 37.5	4.47
32	± 78.125	9.31	± 15.625	1.86	± 18.75	2.24
64	± 39.06	4.66	± 7.8125	0.931	± 9.375	1.12
128	± 19.53	2.33	± 3.90625	0.466	± 4.6875	0.559

at higher gain stages both input channels must be buffered and the ADC does this automatically.

When gain setting is changed it is important to eliminate any offset and gain errors by calibrating the ADC to the current system as the device is calibrated to a gain of 1 by default. Calibration methods and solutions to changing the gain stages are presented in the following chapter 3.2.2. For high resolution ADC it is typical to experience increased code-edge noise, which can cause flickering of several LSBs when the conversion result is close to the code edge. This can typically be reduced or removed with the increased use of sampling of the signal (Maxim Integrated, 2002).

3.2.2 Calibration

Gain and offset registers contain the calibration coefficients for the ADC, which are factory calibrated to a gain of 1. A power-on reset will reset these register values to the factory values, so every setup must be calibrated on every power-on cycle of the device if the setup gain or reference is changed from the default values. The values in these registers can be read by the MCU, so coefficients of a calibrated system can be saved to the EEPROM or other stable storage medium of the MCU from where they can be copied back to the ADC when powering on eliminating the need of calibration when the device powers up. When the ADC is not calibrated for gain

changes the offset errors listed in table 8 can lead to temperature offset of $\pm$ 3 m°C in the case of LMT70 and for PT1000 $\pm$ 6 m°C.

Table 8. Typical offset error for uncalibrated system at every gain stage (AD7124, 2018, Table 3).

	Gain				
	1 to 8	16	32	64	128
Uncalibrated	$\pm$ 15 µV	$\pm$ 12 µV	$\pm$ 6.3 µV	$\pm$ 3.1 µV	$\pm$ 1.6 µV
Calibrated	Order of the input noise				

Internal and system wide zero-scale (offset) and full-scale (gain) calibration modes are provided to change the offset and gain register values automatically. For devices that are operating in a constantly changing environment or when conducting measurements where the front end contains components prone to temperature drift, more frequent system calibrations should be taken instead of relying on one time calibration. For more stable systems a single calibration can be sufficient. Each calibration is completed according to the setup configuration parameters if no changes are made, however improved results are obtained from using lower data rates. Calibration coefficients obtained this way are applicable to any data rate. Considering how system calibration requires both zero scale and full scale values to be applied to the ADC input pins, designing such system might not be practical at every implementation. In cases where system calibration can not be performed, internal calibration can prevent some offset and gain error (AD7124, 2018, Baker, 2006).

If system zero-scale calibration can not be performed due to hardware limitations, chopping of the input channels can achieve equivalent results. When chopping is used the input channels are measured in two configurations by completing a conversion from the positive input to the negative and then internally flipping the input channels, so the negative lead becomes positive and the positive lead negative. This way the system offset V_{OS} is removed when the two conversions are combined. The drawback of this is doubled conversion times, which can be troublesome in certain applications (Sherry, 2003).

3.2.3 Reference

Four different reference voltage sources are available for the ADC to utilize: embedded 2.5 V reference, external REFIN1 and REFIN2 and the analogue side supply voltage. The reference source can be set per each setup so multiple reference sources can be present at the same time.

Both internal and external reference sources are prone to temperature drift, which can directly lead to changes in the conversion results. The AD7124 internal reference offers a typical drift of 2 and a maximum of 15 ppm/°C, which can be considered good for an on-chip reference. For external references similar figures are typical. For references that are generated using excitation current sources the effects of temperature drift are negated as the drift affects the excitation current and the reference voltage drift in an equivalent manner. This behaviour is also known as ratiometric operation. Temperature drift can be avoided by operating the ADC and related components in a temperature stable environment, but this is not always possible. Due to the dynamic input impedance of the REFIN pins when unbuffered, great care should be taken when choosing components to go between the source and REFIN as dc gain errors can occur depending on the source impedance of the reference source. For external references, a low noise reference should be selected.

Typically reference sources can be used to drive low power sensors and circuitry, but the reference load regulation should be considered in that case. The internal reference of AD7124 can drive loads up to 10 mA, but with a load regulation of 50 μV/mA this can lead to a maximum of 500 μV drift in the reference voltage. To negate these problems only small loads should be driven, such as the LMT70 with a typical power supply current of 9.2 μA. In a ratiometric measurement the effects of the reference voltage drop are lesser (AD7124, 2018, Maxim Integrated, 2002).

3.3 Filter register

Several filters are available, five in total, each having different effects on: data rate, settling time and noise rejection. Filter settings can be set per each setup and depending on the filter type selected, they offer great flexibility in terms of configura-

tion. The filters can be split into sinc^4 and sinc^3 filters as shown in figure 3.5 with sinc^4 filters having the longest settling time and best noise performance.

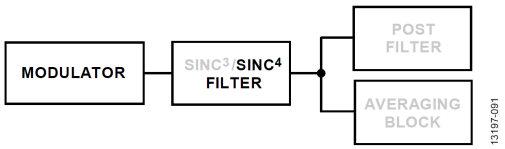

(a) Sinc^4 filter.

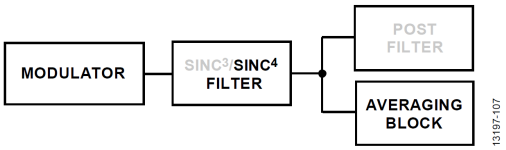

(b) Fast settling sinc^4 + sinc^1 filter.

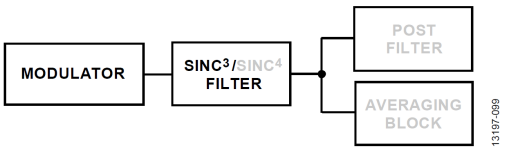

(c) Sinc^3 filter.

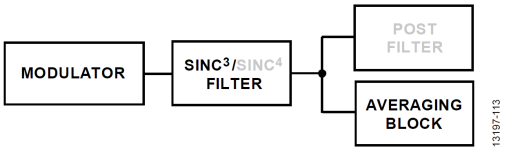

(d) Fast settling sinc^3 + sinc^1 filter.

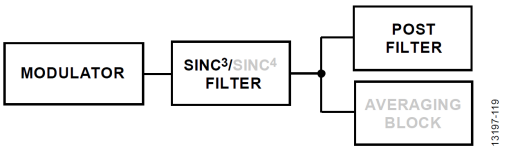

(e) Sinc^3 + post filter.

Figure 3.5. Available sinc^4 and sinc^3 filters, the blocks shown in grey are unused for each configuration (AD7124, 2018, Figures 85, 93, 101, 107, 113).

When conducting measurements with multiple channels, each channel change resets the modulator and filter and the following measurement is delayed by the settling time of the currently configured filter displaying a properly settled result on the ADC output. When multiplexing multiple sensors on the same channel, the changes should be always made with synchronization in mind as due to the nature of the $\Sigma - \Delta$ ADC the weighted average output is still affected by the old sensor results. When changes are made asynchronously a filter dependent number of conversions should be allowed to take place before the output is fully settled and the effects of the previous sensor readings are removed from the weighted result. Depending on the selected filter, one or more intermediate results may be displayed on the output before fully settled result. Depending on the application these intermediate states can be beneficial in determining the changing state of the measured object, but they may not reflect the true nature of the measured value. When conversions are made on a single channel the zero latency mode can be turned on using the SINGLE_CYCLE bit which is enabled by default when using multiple channels, in this mode the conversion time of a single measurements takes roughly the same time as what is the filter settling time. Benefits of this mode are equally spaced

measurements and the limitation of only 1 intermediate results before a fully settled output as shown in figure 3.6, similarly the same effect with zero latency mode occurs on sinc^3 filter (AD7124, 2018).

For noise suppression the first notch of the filter can be set by the filter output data rate select bits for all filters except the post filters, for optimal 50 Hz noise suppression the normal operation SPS should be set at a factor of 50: 1, 2, 5, 10, 25 or 50 for the regular filters and for fast settling filters according to the datasheet so that one of the notches is at 50 Hz. Generally the fast settling and post filters trade noise rejection to decreased settling time, both having a more restricted set of output data rates that are more dependent on the proper first notch location and the power mode being used (AD7124, 2018, Park, 1993).

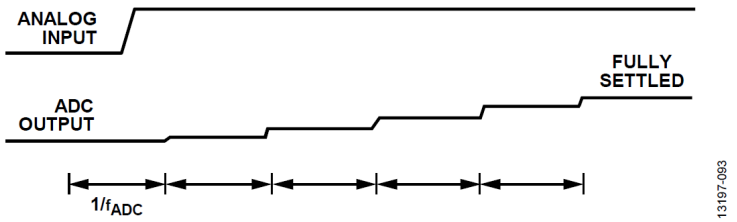

(a) Regular sinc^4 filter. Depending on if ongoing conversion is in progress, fully settled output after 4 or 5 conversions, intermediate results after every conversion.

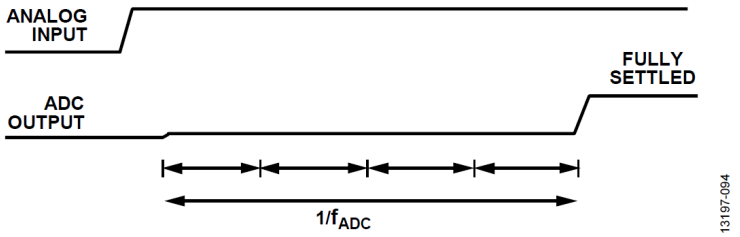

(b) Sinc^4 zero latency filter. Depending on if ongoing conversion is in progress, a single intermediate output is displayed before fully settled output.

Figure 3.6. Asynchronous sinc^4 input with a step change (AD7124, 2018, Figures. 87 and 88). Note how SPS is divided by 4 with zero latency sinc^4 filters, as each conversion is roughly the same as the settling time. Synchronous conversions produce only fully settled results in both modes, similar results can be observed with sinc^3 filters.

3.3.1 Choosing the correct filter

As shown in table 9 the sinc^4 filter has an unmatched noise rejection rate with the disadvantage of long settling time. Considering the slow case sampling rate of 0.1

Hz the main limiting factor is the number of analogue sensors and the measurement offset that can be tolerated from the results. As every conversion takes the complete settling time of the filter to generate an output, to maximize the noise free resolution of the measurements an optimal settling time can be given by

$$t_{settle} = \frac{\frac{1}{f_c}}{n_{sensors}} \tag{4}$$

where t_{settle} is the settling time, f_{c} is the measurement cycle and n_{sensors} is the number of sensors that is going to be measured. This value can be used to calculate the filter output data rate, which in turn will take into account the dead time between channel changes. While this value might give the best noise rejection from the sampling standpoint, in a noisy environment 50 Hz rejection should also be considered and how does the notch settle with the selected filter. Benefits in general noise rejection versus power consumption between low and mid power modes are worth considering when accuracy is of importance, however the increase in power usage when full power mode is used can not be justified for a wearable application.

Table 9. Available filters compared in terms of noise rejection and benefits. Fast settling filters share the same advantages and disadvantages as when comparing between sinc^3 and sinc^4 filters (AD7124, 2018).

Filter type	50 Hz noise rejection [dB]	Advantages	Disadvantages
Sinc^4	120	Best noise rejection	Long settling time
Sinc^3	100	Moderate noise rejection	-
Fast settling sinc^3 and sinc^4	40	Constant settling time	Limited notch position
Post filter	90	Simultaneous 50 Hz and 60 Hz rejection	Limited output data rate

Filter selection for this thesis is made in chapter 4.3.4.

4 Test setup

This chapter details the requirements and implementation of the test setup and the measurement cycles for each sensor. Following aspects are measured: sensor accuracy and repeatability, ADC noise performance with various reference levels and against the reference sensor. Method for two point calibration of the reference sensor is introduced.

4.1 Requirements and limitations

From the sensors detailed in chapter 2 the TMP006 thermopile sensor was decided to be left out from the practical tests due to the difficulties of implementing a working test setup that would be somewhat modular with the other sensors. As all other sensors are based on conducting the heat from the medium of interest to the sensor body, a different type of rigging and medium of interest would be required for the TMP006. As concluded in the chapter 2.4.3 the accuracy of said sensor, and all contactless thermopiles for that matter, is not that great as they exceed the requirements for this sensor study. For the remaining sensors besides the absolute accuracy, most interest is placed on the stability and repeatability of the sensor readings between sensors which is important for heat transfer calculations. As long as similar sensors behave in a similar fashion these calculations are possible. Sensors should have: a predictable time and thermal drift, similar offset and gain errors, and capability of simultaneous measurements.

LMT70 being the most accurate sensor on paper, additional differential measurements were planned with a reference heat flux sensor. By attaching two sensors to each other the temperature difference across a single sensor can be measured, however unclear is how great this change is and how does it correlate with a heat flux flowing through the PCB. Due to the sensors low power consumption the ADC REFOUT pin power delivery is evaluated on one sensor to understand how it affects the measurements. As the internal ADC load regulation is typically 50 µV/mA with a permitted output current of 10 mA, the operating current of a LMT70 should not have any noticeable effects.

As the PT1000 was selected for the reference temperature sensor due to easy interfacing with the bench multimeter, a 3-wire and a Wheatstone bridge measurements were planned to benchmark the ADC capabilities against the reference multimeter. Furthermore the ADC input noise should be evaluated in various reference configurations, as the provided RMS noise and resolution charts on the data sheet are valid for external 2.5 V reference only. ADC is also subjected to similar temperature changes the sensors are experiencing to demonstrate the temperature drift of the ADC and related components.

The room where measurements are conducted has a few limitation that may have adverse effects on the measurements. While the air conditioning unit can be turned off locally to remove the effects of local cyclical heat fluctuations in the room, the building wide ventilation system can not be controlled, and it introduces slowly progressing temperature changes throughout the day.

4.2 The test setup

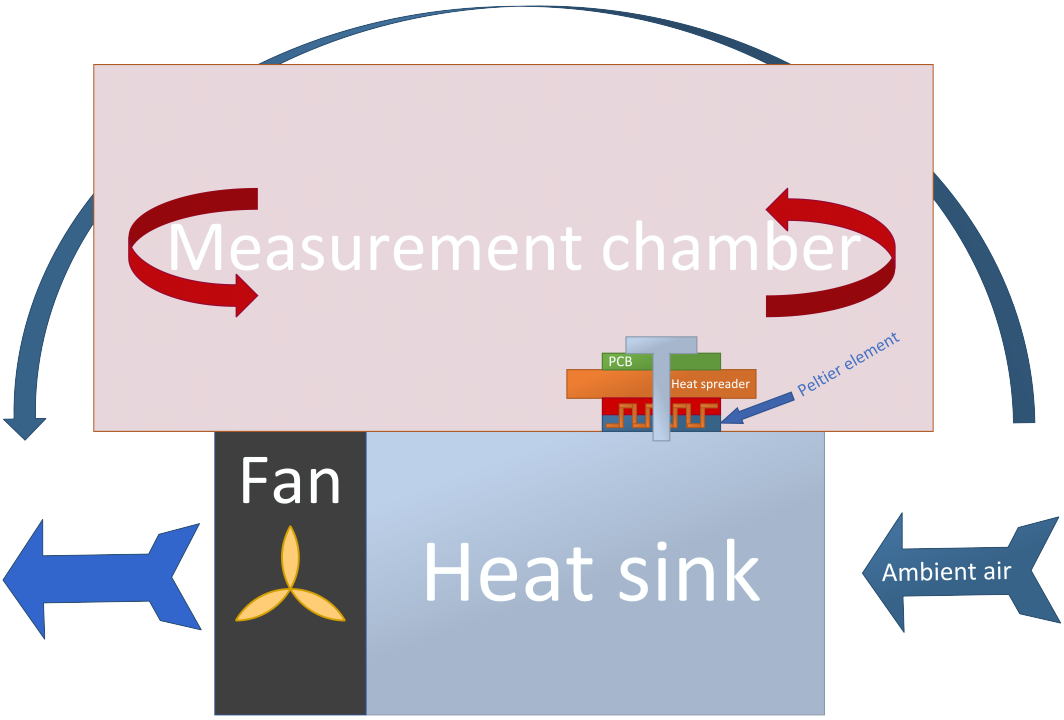

Figure 4.1. Overview of the test setup. Measurement chamber closed off from ambient air changes, inside the DUT PCB pressed against a heat spreader that is cooled or heated by the Peltier device. Ambient air is pulled through a heat sink that is kept at room temperature. Reference sensors are placed on the DUT PCB and in the measurement chamber ambient air.

The physical test setup consists of three parts: The temperature controller, the enclosure and the mounting bracket for the device under test (DUT). Temperature control of the setup is achieved with a TEC1-12715 Peltier device making it possible to heat or cool the DUT at will, a piece of copper is placed in between the DUT and the Peltier device to filter out any small thermal fluctuations caused by the DC power supply and to distribute the effects of the Peltier device evenly in order to avoid any hot spots. An aluminium heat sink with forced convection blowing through it is fitted under the Peltier device to function as a heat sink or radiator depending on the direction of the Peltier device. Due to the constant air flow near the DUT an enclosure is fitted over the heat sink element to block any draft from affecting the DUT when conducting measurements. By eliminating majority of the circulating air around the sensor relatively stable conditions can be achieved inside the enclosure, due to the size of the enclosure low power sensor self heating has minimal effects on the ambient temperature and only external heating element will be the copper block. Temperature reference sensors are placed within the enclosure to measure both ambient temperature and the PCB temperature. The DUT board is tightened against the copper block by using the mounting bracket and some insulating foam to protect any components from direct pressure. The insulating foam acts as a barrier for ambient air changes affecting the immediate area of the sensor. When using sensors that have no PCB a thermal pad is used to improve the thermal contact to the copper block and to provide some cushioning from below for the bare sensor body.

A Y-class PT1000 was selected for temperature reference and ambient temperature monitoring sensor based on the literature review in chapter 2. High stability, accuracy and easy interfacing with a was desirable to avoid any external error sources such as custom circuitry. Two reference sensors are placed in a close proximity of the DUT, preferably mounted on the PCB, two more sensors are used to measure the ambient temperature fluctuations in the test enclosure. On further inspection of the available DMM's it was noted that only the Keysight 34465A supports a PT1000, of which there are two available. Due to this limitation the actual measurements are done with only one reference and ambient temperature sensor. If suitable PT100 sensors or thermocouples were present, the ambient temperature could have been replaced by a Keysight 34461A DMM.

Interference from the MCU is prevented by having no digital communications between the sensors and MCU while the sensors are performing measurements. This should prevent any unnecessary coupled noise from the power lines or communications buses to the sensors.

4.3 Measurements

In a production environment more independent measurement system would be used, but since the reference temperature is sourced from separate devices that don't communicate with the MCU the synchronization of the devices would be difficult. Instead the MCU emulated the automated measurement cycles of the sensors and triggers the reference sources on every beginning of measurement in order to collect as simultaneous data as possible.

The reference DMMs number of power line cycles (NPLC) value is set to 10 for optimal noise suppression without affecting the conversion times too much. Reference measurements are conducted using 4-wire measurements, so input offset removal by auto zeroing between every measurement is not required. With the 10 NPLC setting each conversion will take roughly 200 ms at the expense of noise. Two available excitation currents are available for the 1 kΩ range, normal 1 mA and low power 100 µA. Both current settings are assessed, but manufacturer recommended 100 µA will be followed since the effects of self heating are smaller.

The following chapters detail different sensor measurement cycles and critical configurations.

4.3.1 Reference sensor calibration

A two point calibration will be conducted on the reference sensors: A stirred ice bath at around 0 °C is achieved by filling an insulated container with crushed ice in order to maximize the ice to water surface area. A proper amount of water is added to the container, sufficient to cover half of the ice but not as much so that the ice begins to float. Water level is sustained where the ice doesn't float in order to achieve a stable 0 °C temperature in the water below the ice level.

Second calibration point will be achieved by boiling water to 100 °C and that way two known temperatures are reached without the need of a calibrated temperature sensor. In case of a calibrated sensor a different temperature can be used as well.

4.3.2 TMP117

All the sensors will be pre-programmed with the required configuration data straight into the EEPROM to skip the setup stage when the power is turned on. One device is nominated as ready master and it will be sending data ready interrupts to the MCU through the ALERT pin.

In continuous conversion mode the ready master ALERT pin is connected to the MCU, and all conversions are collected once ALERT pin goes high. Averaging of 8 was chosen to maximize conversion repeatability to ± 1 least significant bit (LSB) and to minimize power consumption, averaging of 32 and 64 are available if required.

To synchronize the external ambient and reference temperature measurements to the test setup logger, one-shot conversion mode was selected instead, and a 1 s conversion cycle was done by the MCU. This way the MCU can trigger both external DMMs and the DUT sensors simultaneously. The sensor will power on to shutdown mode and instead of addressing every sensor individually a mass one-shot mode call can be initiated by making a general-call to address 0000 000 with the eight bit being 0 on the I^2C bus. This wakes up every TMP117 sensor on the bus from shutdown mode ready to respond to a command, by sending a regular write call to configuration register we can set every sensors conversion mode to one-shot conversion. While new conversion is in progress the MCU is free to do other tasks or go to sleep to be awoken by the ALERT interrupt.

4.3.3 HDC2080

Unlike TMP117, the HDC2080 does not support a general-call style mass commanding, so this option does not scale up as well as the TMP117 with multiple sensors. Each sensor must be commanded individually and the measurements will

have a time offset of required configuration time, note that the measurements begin after the device is put into continuous conversion mode and no manual triggering of the measurements is required. Maximum resolution available is used for the measurements.

This sensor goes automatically into low power sleep after every conversion if automatic measurements is not enabled, humidity measurements can be turned off for further power savings. Similar to TMP117, to synchronize the reference and ambient temperature measurements the MCU triggers the sensors at the same time as the DMMs.

4.3.4 ADC

With the ADC multiple aspects are of point of interests: input noise at internal and various external reference voltages, effects of temperature drift on the input channels, and the actual power consumption during conversion and communications. RMS noise tables are presented only for external 2.5 V reference for all power modes. External references could be beneficial when more resolution is required, but without the knowledge of the increased noise on the inputs it is impossible to calculate the effective resolution of the ADC.

In low power mode by setting the sinc^4 filter word to 120 a 5 Hz measurement cycle is achieved with 19.7 noise free bits. This closely matches the DMM NPLC settings giving us similar conversion times. These filter settings apply for all measurements. For mid power tests a filter word of 240 is proposed to achieve similar results. Both filter settings provide exceptional -120 dB 50 Hz suppression.

4.3.5 LMT70

Three sensors were selected to assess multiplexing with the ADC, two are controlled by the logic pins P1 and P2 and one is controlled by the REFOUT pin. All three sensors share the same analogue input channel. Because the control pin changes can not be pre-programmed into the ADC, the pin logic level changes must be done by the MCU after each individual measurement bringing some unnecessary

communications between the MCU and ADC. Since every measurement is a separate single conversion there is no need to reset the modulator and filter in between measurements, as writing into the mode register achieves this at the start of every conversion.

Based on the output voltage of the sensor within the measurement range, gain stage of 2 was selected for the initial starting point in order to not spoil the measurement results with any external circuitry. With the internal reference and a unipolar measurement a theoretical noise free resolution of 1 mK per 3 bits is achieved and the gain stage limits the operation of the sensor to -30 °C which is more than suitable for the case requirements.

Fourth sensor is attached on top of a PCB mounted LMT in an attempt to measure the top side temperature of the LMT. In such experimental setup the goal is to be able to measure the heat flux that is affecting the DUT by conducting a differential measurement between the two sensors. A reference heat flux sensor will be mounted on the PCB for comparison. Appropriate gain settings will have to be found through experimentation, gain setting of 128 will allow up to 4 °C temperature difference between the two sensors before clipping which is a good starting point.

4.3.6 PT1000

The initial assumption is that from a power usage standpoint the manufacturer recommended test current of 100 μA is too high for wearable applications when compared to other solutions available, however since the PT1000 acts as the reference temperature sensor using the same sensor on the ADC would give great insight on the performance parameters of the ADC and how does it compare to the DMM in terms of noise. Two different styles of measurements are conducted: a 3-wire measurement with a ratiometric bias current generating the reference voltage, and a Wheatstone bridge with a dedicated external reference voltage source.

Based on simulations the voltage across the bridge for a temperature range of 0 to 50 °C is roughly 20 mV with a 0.5 V voltage source, so a gain of 16 should be used. The current running through the PT1000 is over double the manufacturer recommended 100 μA so slightly more self heating effect is expected; however the

excitation voltage can not be lowered more as the ADC reference minimum voltage limit is 0.5 V.

For the 3-wire measurement the manufacturer recommended 100 μA excitation current is exceeded to match the Wheatstone bridge current of 250 μA, so the SHE is similar in both measurements. The same excitation current will generate the reference voltage for the ADC, making the measurement ratiometric and thus removing the effects of excitation current drift or inaccuracy. Two different reference voltage sources are planned, 2.5 V and 0.6 V, to assess different measurement ranges. The maximum voltage over the PT1000 over the temperature range of 0 to 50 °C will be 300 mV, which is suitable for gain ranges of 8 or 2 depending on the reference voltage (Pertijs and Huijsing, 2006).

Both PT1000 circuits utilize the togglable PSW pin on the ADC, which is a configuration controlled switch between the PSW pin and analogue ground. Turning the switch off allows a portable device to cut off the power consumption of the passive PT1000 circuits when they are not in use. For the 3-wire measurement cutting off the excitation current supply is also an option.

5 Circuit and PCB layout design

Four PCBs were designed to accommodate all the planned measurements detailed in chapter 4: independent digital sensor board, modular ADC board and two analogue sensor boards. As a cost saving measure the two analogue boards were manufactured onto the same PCB with complete isolation from one another.

5.1 General considerations

Sensor boards were made as 4 layer PCBs so all the signals and VCC can be sandwiched between the top and bottom ground planes to minimize the effects of noise that could couple to the board. To minimize the thermal resistance between the top and bottom layers, internal copper polygons were created in signal and power supply layers under the areas where sensors are located and the area surrounding sensors was populated with vias. Due to manufacturing reasons vias were not filled, which would have lowered the PCB side-to-side thermal resistance even further. Due to the lack of calibration equipment sensor thermal pads were left unsoldered at the expense of increased thermal resistance, as soldering them can cause internal stress within the sensor package which can lead to unpredictable measurement errors as shown in figure 2.12. Bottom side of the boards was left without solder mask to expose the bare copper and to provide an optimal thermal contact with the copper block attached to the heating element. Thermal interface between the PCB and copper plate were thought about and ultimately it was decided that bare copper on copper is sufficient as all measurements are conducted on the top side of the PCB. This thermal interface will cause sub-optimal responsiveness from the PCB measurements but since no rapid temperature changes are required for this stage of testing the bare contact will suffice.

5.2 Digital sensor board

Dedicated PCB was designed for the selected TMP117 and HDC2080 sensors with a separate NCP160 3.3 V low-dropout regulator (LDO) with high PSRR, low noise,

and capability to source a maximum of 700 mA (NCP160, 2021). Required level shifter for bi-directional communications was selected and the I^2C pull-up resistors were placed near the level shifter, as far as possible from the sensors, to avoid any external heating of the board around the sensor area (PCA9306, 2019). Suitable area of low thermal resistance was prepared near the sensors for a reference temperature sensor. Considering the HDC2080 is primarily a humidity sensor the manufacturer recommends of thermally isolating the sensor from the PCB to not spoil the humidity measurements with heat conducting from and through the PCB. For the temperature measurements of this thesis this guideline is dismissed to improve the thermal conductance to the sensor.

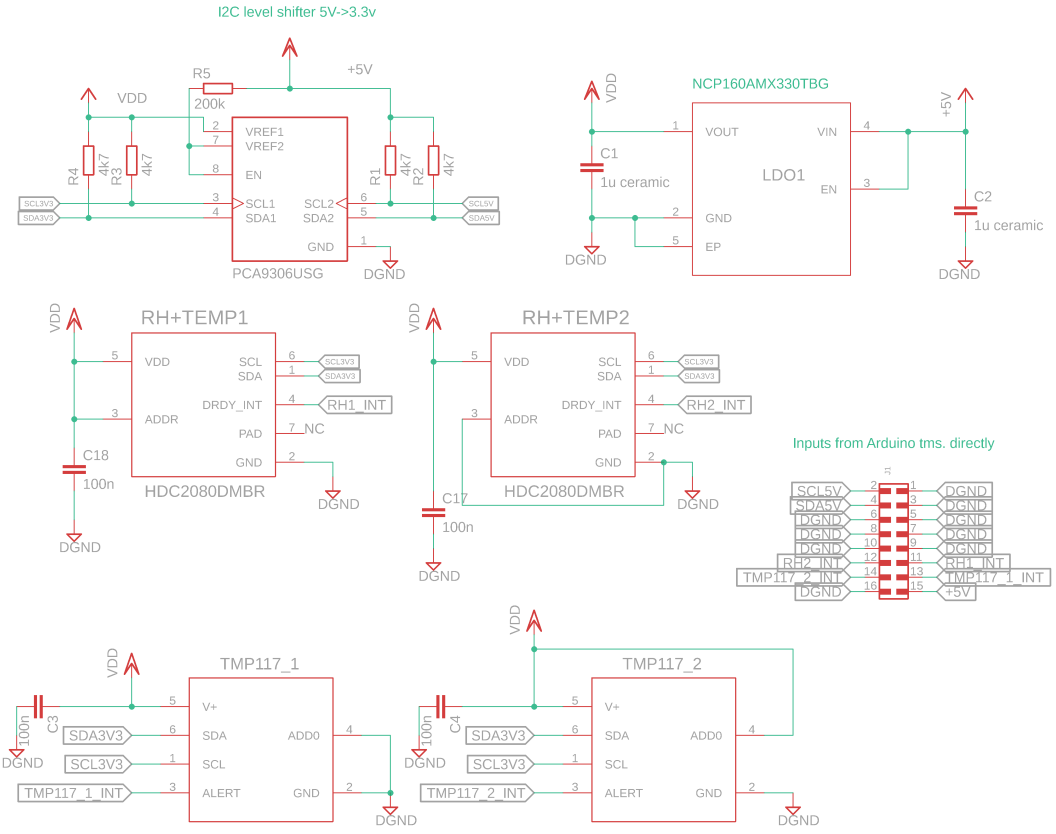

Figure 5.1. Schematic for the digital sensor board. LDO, level shifter and two TMP117 and HDC2080, larger schematic can be found in appendix 3.

Sufficient bypass and decoupling capacitors were placed for the sensors and the LDO regulator (HDC2080, 2021, TMP117, 2021, NCP160, 2021). Individual interrupt pins were brought over to the MCU for maximal flexibility.

5.3 ADC board

ADC board was split in two distinct sides: digital communications on one side of the PCB; analogue signals, power delivery and the ADC itself on the other side. Two LDOs are used: one for the ADC, and another dedicated for external sensors. If required, the possibility of using either LDO for external sensor boards was made possible. A shunt resistor was installed for the ADC LDO for the possibility of current monitoring.

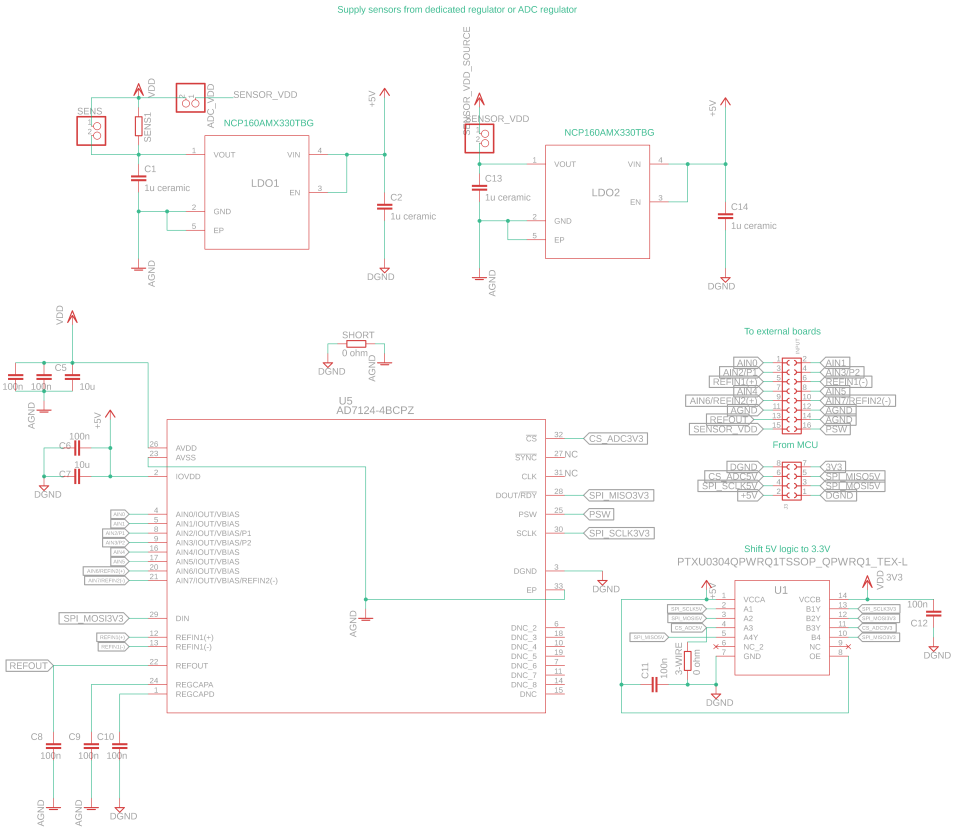

Figure 5.2. ADC board schematic with two optional power supplies, communications level shifter and all necessary pins routed to the external board connector. Larger schematic can be found in appendix 4.

A SPI voltage level translator was intended to be used in the design, but due to the global component shortage this voltage level translator never arrived. Instead a bi-directional level shifter was constructed out of discreet components on an external breadboard between the MCU and the ADC board. This was seemed fit for the intended purposes of this test setup, as the SPI clock speeds can be kept low enough to not introduce any significant signal distortion in the SPI lines.

For maximum modularity, all necessary ADC pins were made available on the ADC board connector so the designed PCB could be used for other measurements not re-

lated to this thesis. The only limitation for additional sensor boards is the 250 mA output current of the LDO, but technically this can be circumvented by connecting any power supply to the SENSOR_VDD connector and thus feeding the external sensor board through the ADC board connector. Care should be taken when operating the ADC board jumpers, as there is no reverse polarity protection for external power supplies.

Due to a design oversight the $\overline{\mathrm{SYNC}}$ pin was left unconnected, making external reset of the modulator and filters impossible without register writes. For the purposes of this thesis this is not a problem since multiplexing of sensors is achieved through the ADC logic pins that require single conversion mode, but it is something to be considered for the future use of this design.

5.4 Analogue sensor boards

Two separate analogue boards were designed due to the lack of available channels on the selected ADC and to simplify the PCB design. One board for PT1000 measurements for both 3-wire configuration and a Wheatstone bridge. Another board for LMT70s where multiple sensors are controlled using the ADC I/O, one sensor being powered by the ADC and an experimental setup for measuring HF using two LMT70 sensors that are attached to each other.

5.4.1 LMT70 board

Two output channels with four sensors in total, sensors 1-3 acting as multisensory array all sharing the same ADC input and external sensor 4 having a dedicated input channel for differential measurements. Sensors 1,2 and 4 are controlled using the two digital IO capable pins of the ADC, sensor 3 is powered and controlled with the controllable ADC reference source output and sensor 4 shares the control pin with sensor 2 for differential measurements. Bypass capacitor was fitted for each sensor and both output channels were fitted with 330 pF filter capacitor. According to manufacturer the LMT70 output pin can drive capacitance up to 1.1 nF without the aid of series resistor for stable signal (LMT70, 2015).

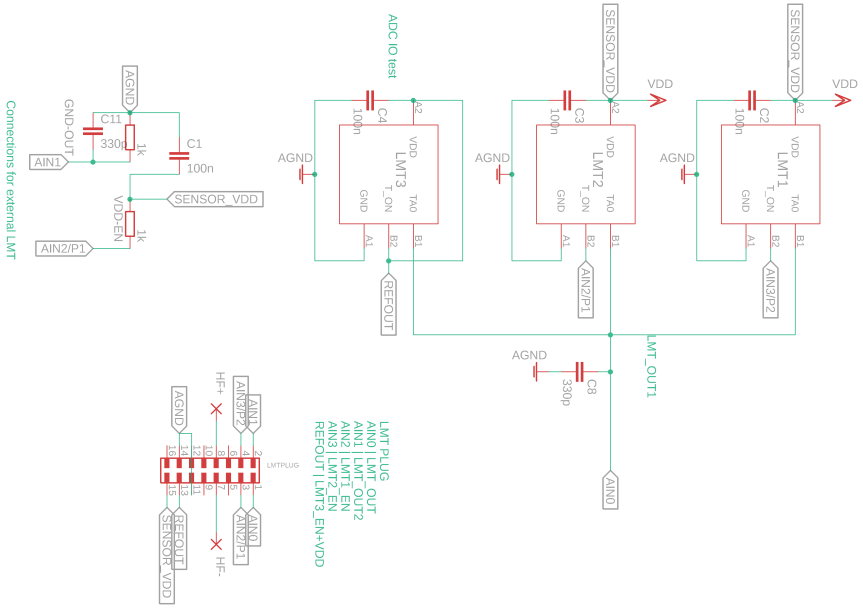

Figure 5.3. Schematic for the sensor board. Two signal outputs and four LMT70 sensors. Three mounted on the board and one external with a footprint made of dummy resistors. Larger schematic can be found in appendix 5.

The REFOUT pin on ADC which is used to power sensor 3 can supply a maximum of 10 mA of current with a load regulation of 50 µV/mA. LMT70 draws a maximum of 12 µA of current, which leads to a maximum of 0.6 µV variation in the internal ADC reference. The data sheet specification for internal reference variation is 2.5 V $\pm$ 0.2% which is 5 mV, so the deviation caused by one sensor is negligible. Due to misinterpretation of the data sheet, ADC REFOUT pin was not a togglable pin in a sense that in order to turn the REFOUT pin off, the internal reference source must be also completely turned off. In the circuit designed output AIN0 is constantly occupied by sensor 3, unless internal reference is turned off in which case no further measurements can be made in the absence of reference voltage to the ADC. To alleviate the problem, multichannel measurements were conducted using only sensors 1 and 2 with the REFOUT pin being physically disconnected from the sensor board.

Suitable connecting points were prepared for the external LMT70 using dummy footprints in the schematic, the sensor was attached on top of the LMT2 by using thermally conducting glue and attached to the PCB by hand. Area of low thermal resistance was prepared for the reference heat flux sensor.

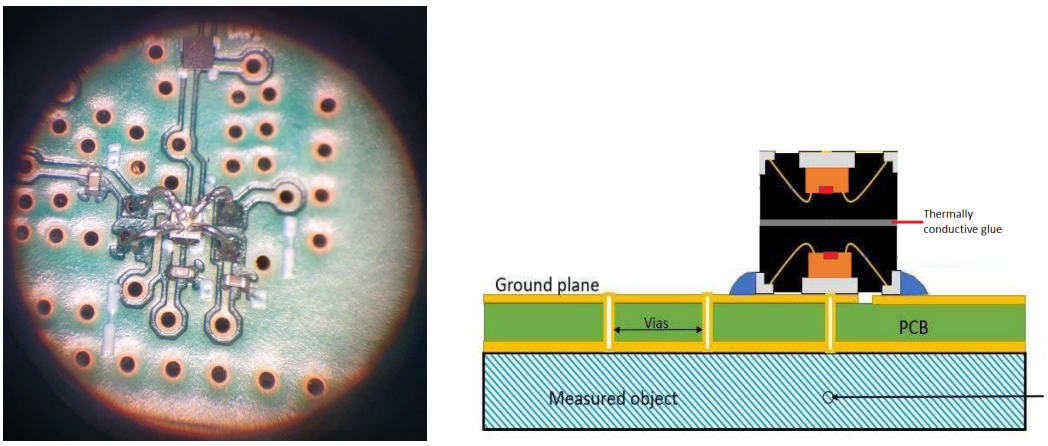

(a) Mounted on the PCB upside down.

(b) Illustrative drawing of the two LMT70s, thermally conductive glue between the two sensors.

Figure 5.4. Layout for two LMT70s stacked on top of each other to measure the transmitted heat flux.

5.4.2 PT1000 board

Three measurements in total are conducted using the PT1000 board, two different style of temperature and one where ADC input noise is measured using two external references of 0.6 V and 2.5 V at various gain and filter settings.

The bridge consists of three low tolerance and temperature coefficient resistors and the PT1000. Using a 0.5 V ADR130 precision voltage reference source the Wheatstone bridge is powered and ADC external reference is set to 0.5 V, considering the bridge draws a nominal current of 500 µA and the source has a $\pm$0.13 mV/mA load regulation no significant change is observed when the initial accuracy of $\pm$ 1,75 mV of the source is taken into account. For ADR130 input side capacitors are not required, but 1 µF and 100 nF smoothing and bypass capacitors were placed. Similar values were placed on the output side, although big transients are not to be expected with this circuit (ADR130, 2018).

3-wire measurement is conducted in a ratiometric fashion, where 2.5 V and 0.6 V references are set by the excitation current that is used to drive the PT1000. Second excitation current is provided for the negative input lead to cancel any lead error voltages by closely matching the positive and negative lead routes on the PCB.

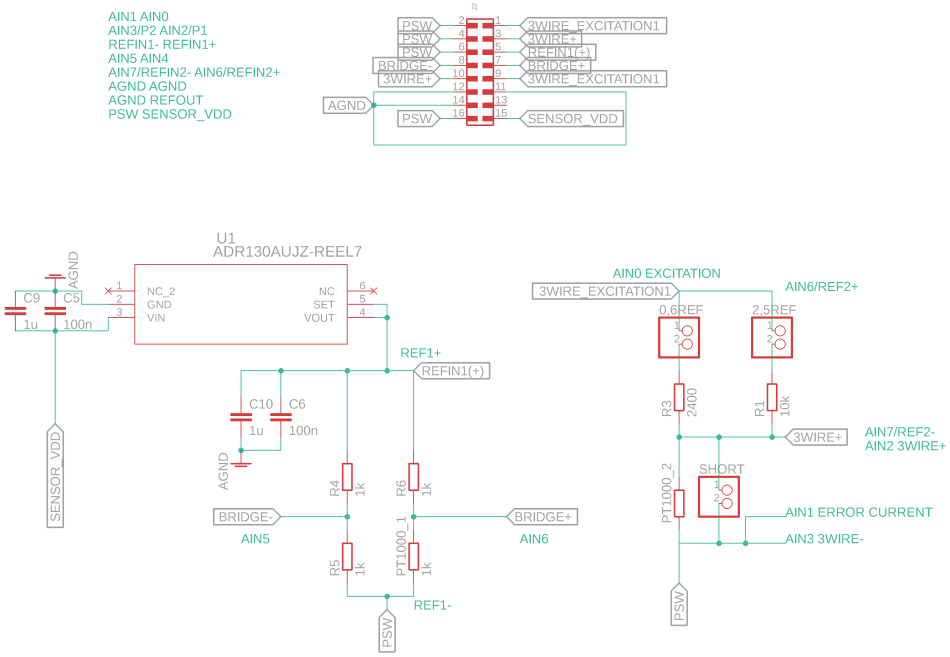

Figure 5.5. Schematic for two PT1000 measurements using 3-wire and Wheatstone bridge. Both circuits are connected to the controllable PSW pin of the ADC, which can be toggled on and off using software. Larger schematic can be found in appendix 6.

6 Tests

Measurements were conducted on the reference sensors and the three selected sensors over a temperature range and the results were logged. Due to sudden malfunction of the ADC board the PT1000 and ADC input noise measurements were not completed.

6.1 Reference sensor

Three separate measurements were conducted on the reference sensors: 0 °C offset calibration, case requirement temperature range offset and sensor self heating effect measurement.

The two sensors were placed in an ice bath close to 0 °C and the offset deviation between the two sensors was observed to be around 0.055 °C as seen from figure 6.1.

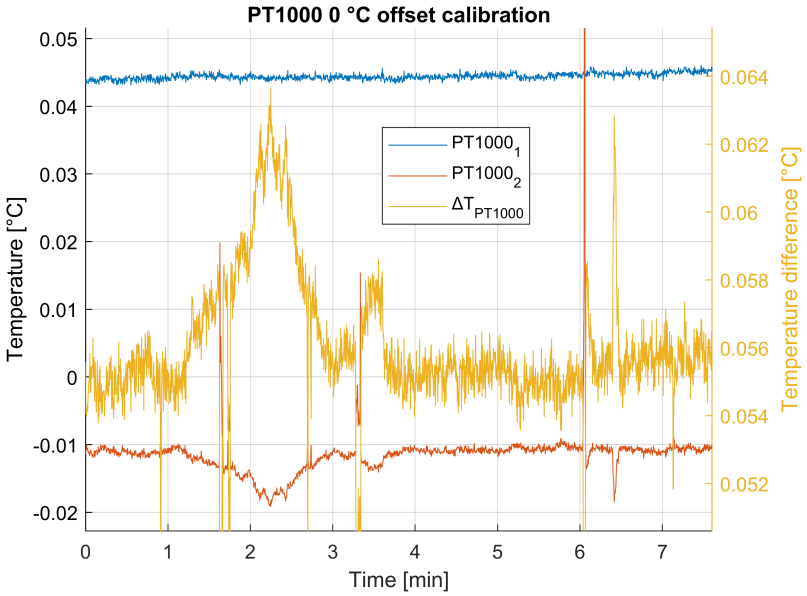

Figure 6.1. Two sensors placed in a 0 °C ice bath, temperature offset is observed to be around 0.055 °C. Sensor 1 readings are stable, however sensor 2 readings contain a few glitches that are most likely caused by movements due to external factors.

A temperature cycle of 20 - 50 °C was conducted at roughly 10 degree separation to monitor the temperature offset between the two sensors for the intended test temperatures. The two reference sensors were observed to behave in a similar manner

through out the complete temperature range with minimal temperature drift when compared against each other. Sensor 1 was selected as the PCB reference and sensor 2 as the ambient temperature monitoring sensor.

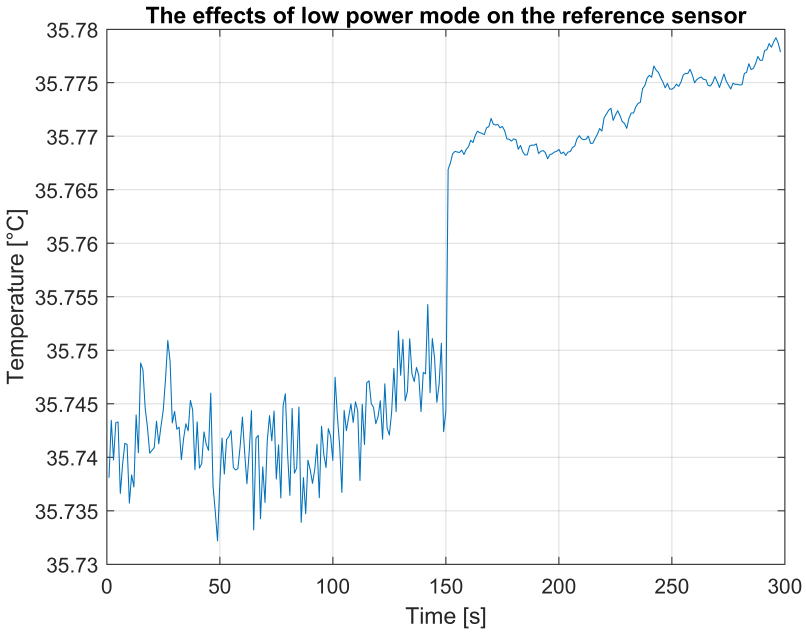

Figure 6.2. By turning the low power mode off for the reference sensor at 150 seconds an instantaneous shift and filtering effect can be observed from the results. Nominal self heating error of 1.43 mK for 100 µA and 143 mK for 1 mA excitation currents is given by equation 5.

The sensor self heating effect can be observed when the excitation current is increased beyond manufacturer recommended values. A 1 mA current introduces filtering to the sensor as the sensor body is constantly heating up as seen in figure 6.2.

The magnitude of the self heating temperature error is given by

$$\Delta T = \frac{RI^2}{E} \tag{5}$$

where ΔT is the temperature error, R is the resistance of the sensor in kΩ, I is the excitation current in mA and E is the self heating coefficient which for a 5.0 x 2.0 x 0.63 sensor is 7 $\frac{mW}{K}$ when the sensor body is surrounded by air. When the excitation current is increased by x10, the self heating effect increases by x100.

6.2 Practical tests on sensors

Test sequence ranging from room temperature to 45 °C was conducted by increasing the heating element current at incremental steps and letting the test setup temperature settle. After a suitable time current was further increased, until the setup reached roughly 45 °C. Measurements were logged by the two reference DMMs controlled by the MCU and by MCU relaying the received data to a simple python data logger.

The measurement sequences were assessed individually with digital sensors and the ADC, and a conclusion was made that they can be combined to make the measurement process more efficient. Major risk of contaminating the received data by digital communications was noted, but in testing no noticeable changes were detected. Communications between the sensors or the ADC were conducted only after all measurements including the DMMs were completed.

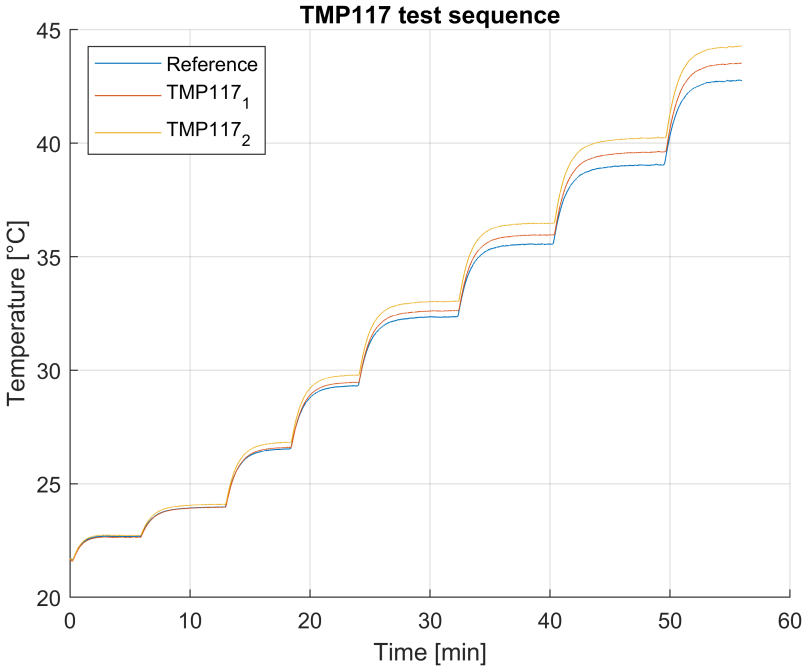

Figure 6.3. TMP117 test sequence with two sensors and a reference, drift can be observed at higher temperatures.

From the TMP117 measurements presented in figure 6.4 a great initial accuracy can be observed, where the two sensors are within 0.1 °C of each other, which can be considered great result for this sensor. However as the copper block heats up the gain starts to dominate between the two sensors and the results drift apart. From the initial condition where the sensor separation is 0.1 °C and the sensors are showing

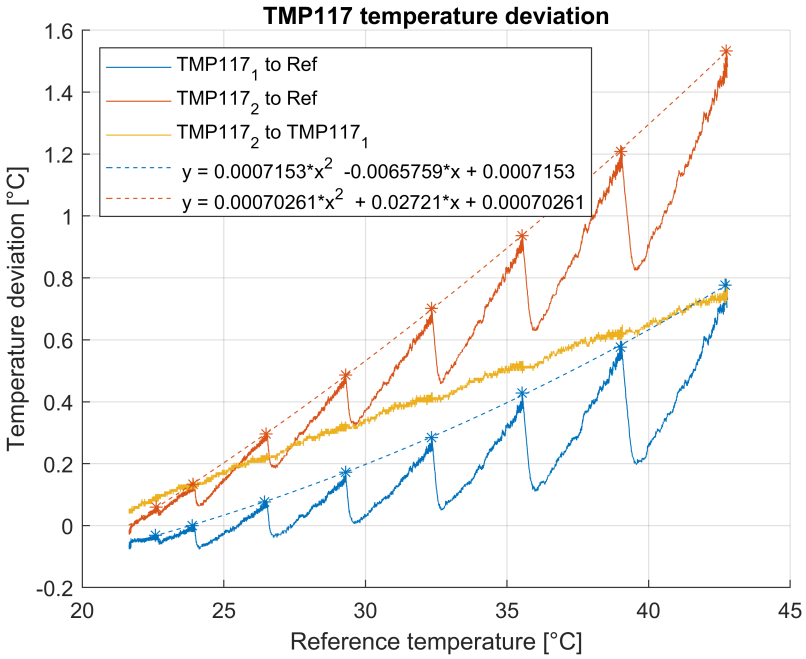

Figure 6.4. Temperature deviation between TMP117 and the reference, gain and offset error can be observed. Possible cause is soldering induced stress. Sharp downwards changes in the deviation figure are caused by the DUT sensors lagging behind the reference sensor causing a momentary decrease in the deviation to reference.

almost exactly the reference value, sensor 2 being around 0.01 °C off and sensor 1 being around 0.05 °C off, the gain error ramps up fairly linearly and at 43 °C object temperature 0.8-1.5 °C deviation can be observed. One probable cause for this gain error could be internal heat related stress from the soldering process, but this can not be confirmed at this time.

Surprising results was obtained from the HDC2080 in terms of temperature matching between sensors, where the temperature deviation was less than 0.6 °C through out the whole temperature range as seen in figure 6.6. The sensors had a significant offset error at the initial conditions which slowly approached the reference temperature. While gain error is present, it's not as prominent as with TMP117.

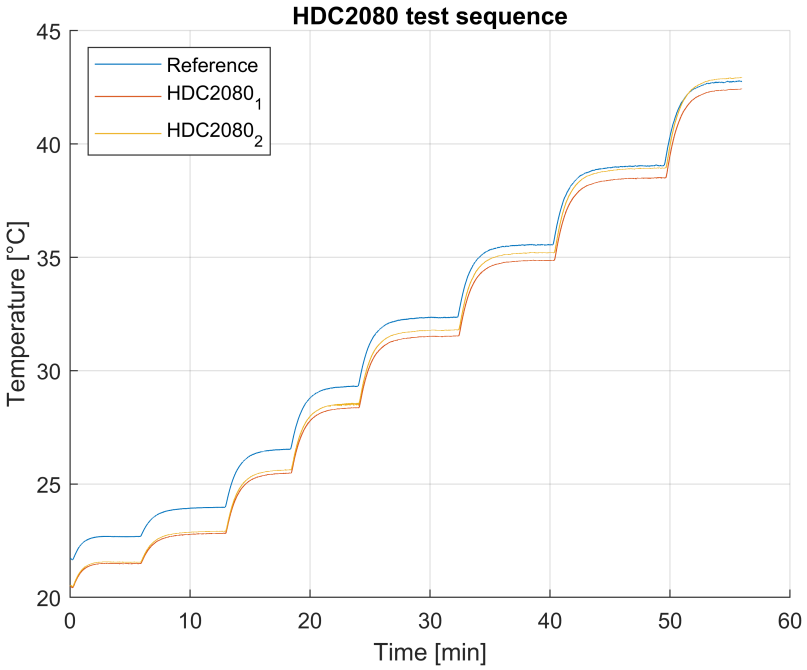

Figure 6.5. HDC2080 test sequence with two sensors and a reference. Initial offset error is observed, gain error is present while not as prominent as with TMP117.

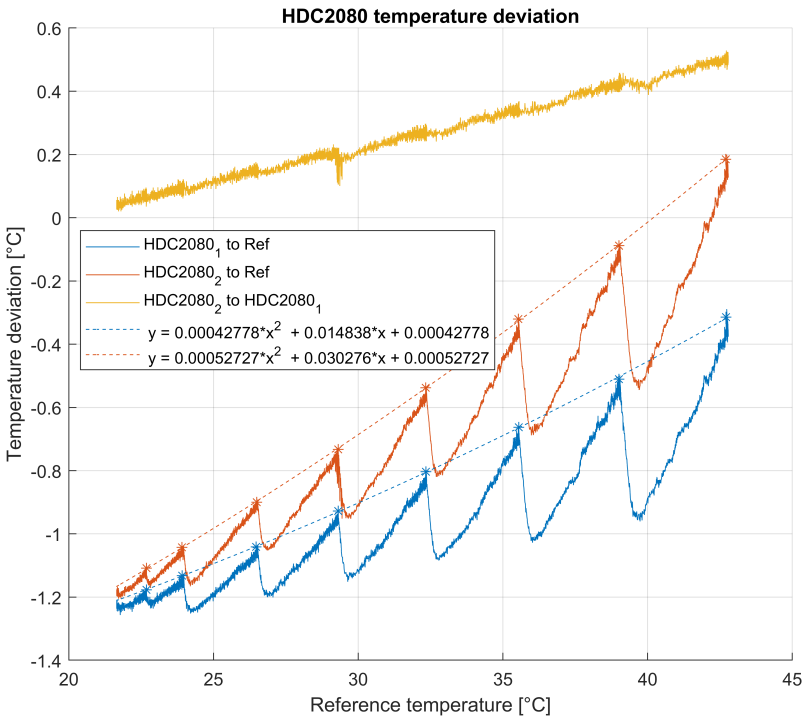

Figure 6.6. Temperature deviation between HDC2080 and the reference, slight gain and significant offset error can be observed. Sharp downwards changes in the deviation figure are caused by the DUT sensors lagging behind the reference sensor causing a momentary decrease in the deviation to reference.

LMT70 was the most accurate and best performing in terms of temperature matching between sensors according to the manufacturer and results supporting this were obtained. Initial accuracy was good when compared against the reference sensor and while the sensor did drift away from the reference the sensors kept together well as shown by the figure 6.8. The overall temperature difference between the sensors across the whole temperature range was less than 0.15 °C, even when considering that the $LMT70_2$ had an another LMT70 glued on top of it so the comparison was not between two identical sensors. This additional LMT could also be the cause for the slight gain error making the two sensors drift apart.

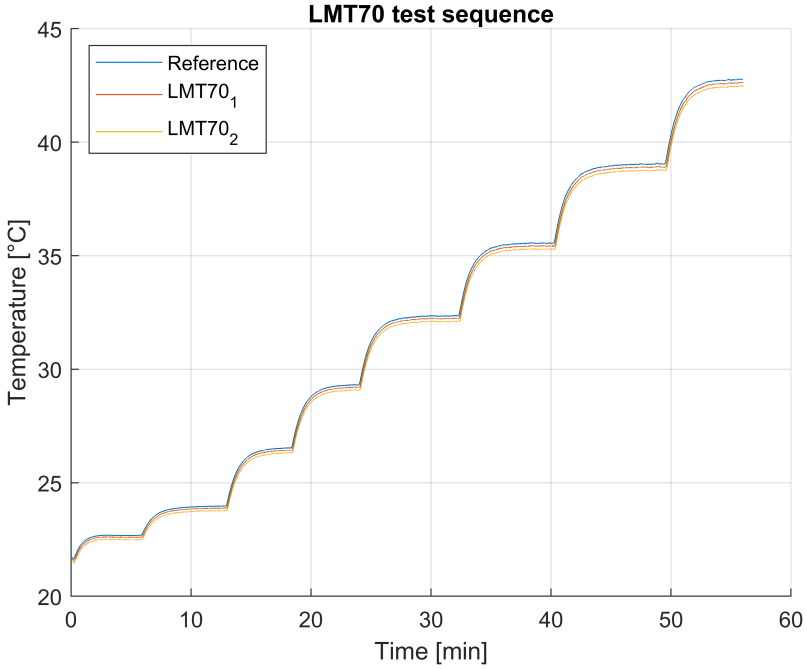

Figure 6.7. LMT70 test sequence with two sensors and a reference. Minor drift is observed at higher temperatures.

The effects of ambient temperature were observed to have a direct relation to the deviation between each sensor pair, presented in figure 6.9. All sensor pairs responded to the changes in ambient temperature in a linear manner, TMP117 matching the changes almost exactly.

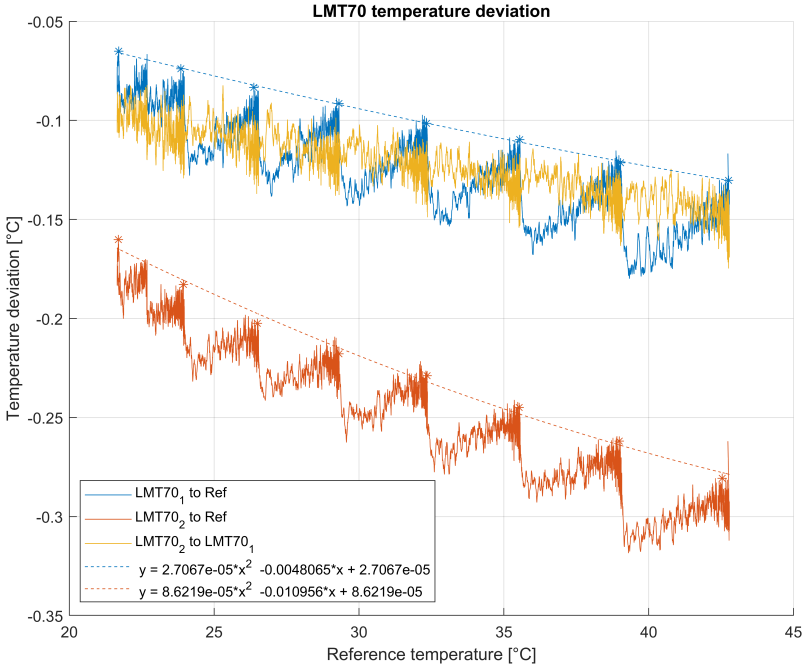

Figure 6.8. Temperature deviation between LMT70 and the reference, deviation between the two sensors is observed to be fairly constant. $LMT70_2$ is the sensor which has another LMT70 glued on top of it, which might explain the increased gain error compared to the other LMT.

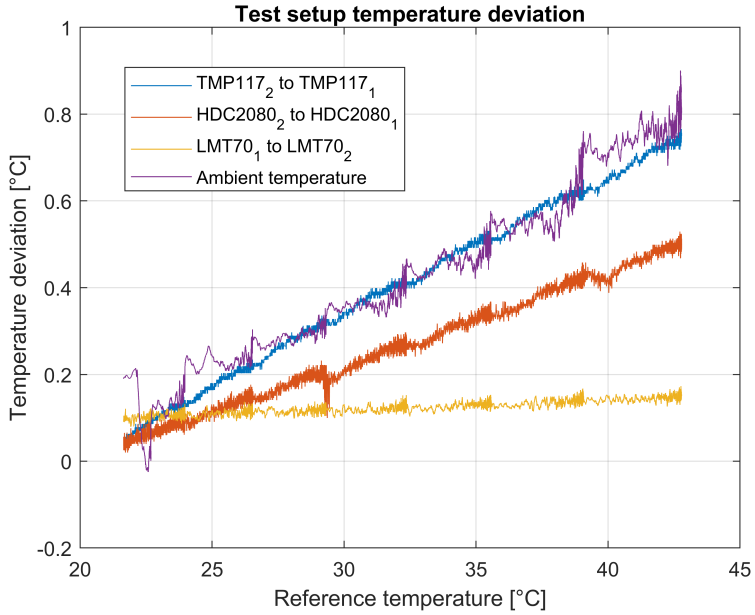

Figure 6.9. Sensor pair deviations and the change in ambient temperature. Clear correlation can be seen, but it is uncertain is it directly caused by the ambient temperature change or are the sensors self heating. Further tests need to be done with the relation of sensor results and ambient temperature.

7 Results and discussion

In this master's thesis temperature sensors suitable for human biosignal measurements was studied. A literature review was conducted, and four sensors were selected as the most promising candidates, preliminary measurements were performed to further study the initial accuracy and the measurement deviation of the sensors from the same manufacturing batch. Evaluation of the performance of sensors is done and suggestions for improvements to the test setup are presented.

Based on the sensor tests the LMT70 is the preferred sensor. From the manufacturer provided data the TMP117 should have better performance than the HDC2080 in every aspect except power consumption but the measurements do not support this. From power usage standpoint TMP117 could be the better choice over LMT70, if it performs according to the manufacturer specifications.

Due to time constraints all planned measurements were not completed and some initial test sequence results became the final results as the ADC malfunctioned without a clear cause. Many aspects that were previously unknown are now better understood and the foundation is set for further use of the devices presented in this thesis.

7.1 Practical considerations

For accurate and responsive temperature measurements the temperature path from the medium of interest to the sensor must be carefully considered. Thermal mass should be minimized, and thermal conductivity should be maximized. Thermal path within the PCB should be considered regardless of are the measurements conducted through the PCB or by direct sensor contact to the subject.

When operating a wearable device the available power is limited promoting the use of low power peripherals and power saving techniques to maximize the operating time of the device. Based on the literature, measurement sampling should be calculated in a way that minimizes the available measurement data without sacrificing meaningful results. Independent operations from the MCU should be favoured to keep the MCU in a standby state acting only as gateway between the completed

conversion results and a storage medium.

While the number of available sensors increases drastically multiplexing must be practiced for both analogue and digital sensors. For the digital sensors the available addressing space, whether implemented in software or hardware, is the limiting factor. With analogue sensors the available input channels of an ADC is the limiting factor, from manufacturing cost standpoint having multiple ADCs can be problematic. With a single ADC and multiple multiplexed inputs the conversion result time drift is inevitable. Truly simultaneous conversion results can only be achieved by multiple ADCs capable of syncing to a common signal. ADC operations was investigated in detail and key features of the device was presented. For single channel measurements the selected ADC may be excessive due to the number of unused channels and available features focused on multi channel operations. However the configurable input filter and low power operations are optimal for wearable use.

Several sensor types were evaluated and sensors with good output linearity and high repeatability were favoured in the selection process. Mechanical stress caused by the thermal variations occurring in PCB assembly was considered as one of the major threats to measurement integrity and it could be the cause for the subpar results obtained from the digital sensors in this thesis.

7.2 Sensor tests

The reference sensors initial 0 °C offset was observed to be within 0.055 °C with both sensors being well within the manufacturer declared range. Measurement cycle temperature range was run in the test setup and the sensor deviations were logged. No significant drift was observed between the two reference sensors, which would indicate that the two sensors are functioning identically across a temperature range.

Based on the measurement results all sensors had an increasing gain error as the object temperature rises. Some of the drift could be attributed to the reference sensor as the actual behaviour of the PT1000 is not known, however similar reference related error would be present in all measurements making the comparison between the different sensors still valid. Sensor SHE could be another aspect skewing the

results, if the sensors are not heating up equally. As the short term behaviour of the sensors is predictable, a polynomial can be fitted to the results and the results could be corrected with the help of a calibrated reference sensor. Long term behaviour was not studied due to time constrains. Ideally the sensor to sensor deviation would be a horizontal line indicating how the two sensors are behaving identically, a feature that can be seen from the LMT70 measurement results.

The effects of ambient temperature changes were observed on the sensor result deviations, but direct relation can not be stated at this time. Further measurements with stable conditions where only the ambient temperature changes would be required.

7.3 Test setup considerations

While the test setup had promising design aspects, it was quickly noted how the environment was not suitable for determining any meaningful results from the resolution capabilities of the various sensors as even with an enclosure the ambient effects on the sensors were severe. During measurements it was noted how the presence of one or more persons within the line of sight of the enclosed test setup was enough to increase the reference temperature readings. A temperature controlled cabinet would be the preferred method for further tests.

7.4 Future work

Several measurements were not completed even though they were originally planned, and the physical boards exist. Some were due to time constraints, and some were due to problems with the ADC refusing to communicate. Some tests were originally planned but scrapped from the scope of this thesis due to an effort of keeping the thesis in reasonable limits.

One of the main points of interest was the ADC input noise levels at various reference, filter and power mode settings which requires more practical tests and research. PCB exists with the capability of shorting the ADC inputs with options for external reference sources. Since practical tests on the ADC fell short of the original goals, no power consumption measurements were conducted, and data sheet values

were used instead for measurement cycle power estimation.

TMP117 results were surprising in the magnitude of the temperature deviation that was measured, and further testing is needed before the sensor performance is declared to be below manufacturer specification. The effects of soldering shift could have skewed the results and new tests should be performed where extra caution is taken for avoiding thermal stress on the sensor body during assembly. Similarly the effects of ambient temperature for all the sensors and especially for TMP117 should be further researched as a clear relation was found but it could not be confirmed.

Original sensor selection included the contactless thermopile TMP006 for temperature measurements which was ultimately removed from the test sequence due to being so far outside the sensor specification set for this thesis, however contactless sensor performance should be researched more for any hidden potential.

The case requirements for this thesis were shown to be exceedingly difficult to fulfill with readily available sensors and not a single sensor met them, for further tests the characteristics of the signals being measured should be studied more in order to determine the requirements for measurement accuracy and resolution.

References

AD7124 (2018), *AD7124-4 datasheet*, Analog Devices. Revision D.
URL: *https://www.analog.com/media/en/technical-documentation/data-sheets/AD7124-4.pdf*

ADR130 (2018), *ADR130 datasheet*, Analog devices. Revision D.
URL: *https://www.analog.com/media/en/technical-documentation/data-sheets/ADR130.pdf*

Bacciarelli, L., Lucia, G., Saponara, S., Fanucci, L. and Forliti, M. (2006), Design, testing and prototyping of a software programmable I2C/SPI IP on AMBA bus, Ph.D. Research in Microelectronics and Electronics.
URL: *https://doi.org/10.1109/RME.2006.1689973*

Baker, B. (2006), *A Glossary of Analog-to-Digital Specifications and Performance Characteristics*, Texas Instruments. Application report SBAA147, revision 10/2011.
URL: *https://www.ti.com/lit/pdf/sbaa147*

Batagelj, V., Bojkovski, J. and Drnovšek, J. (2003), 'Methods of reducing the uncertainty of the self-heating correction of a standard platinum resistance thermometer in temperature measurements of the highest accuracy', *Measurement science and technology* **14**(12), 2151–2158.
URL: *https://doi.org/10.1088/0957-0233/14/12/016*

Bui, N. T., Vo, T. H., Byung-Gak, K. and Oh, J. (2019), 'Design of a solar-powered portable ecg device with optimal power consumption and high accuracy measurement', *Applied sciences* **9**(10), 2129.
URL: *http://dx.doi.org/10.3390/app9102129*

Charlton, M., Stanley, S. A., Whitman, Z., Wenn, V., Coats, T. J. and Thompson, J. P. (2020), 'The effect of constitutive pigmentation on the measured emissivity of human skin', *PLoS One* **15**(11).
URL: *https://doi.org/10.1371/journal.pone.0241843*

Childs, P., Greenwood, J. and Long, C. (2000), 'Review of temperature measurement', *Review of Scientific Instruments* **71**(8), 2959–2978.
URL: *https://doi.org/10.1063/1.1305516*

Childs, P. R. (2001), *Practical Temperature Measurement*, 1 edn, Butterworth-Heinemann.

Cuadras, A. and Casas, O. (2006), 'Determination of heart rate using a high-resolution temperature measurement', *IEEE SENSORS JOURNAL* **6**(3), 836–843.
URL: *https://doi.org/10.1109/JSEN.2006.874445*

Goldsmid, H. J. (2016), *Introduction to Thermoelectricity*, 2 edn, Springer.
URL: *http://dx.doi.org/10.1007/978-3-662-49256-7*

HDC2080 (2021), *HDC2080 datasheet*, Texas Instruments. Revision C.
URL: *https://www.ti.com/lit/ds/symlink/hdc2080.pdf*

Hurley, R. B. (1958), *Junction transistor electronics*, 3 edn, John Wiley and Sons.

Immonen, A. (2019), A heat flux sensor test setup, Master's thesis, Lappeenranta-Lahti University of Technology LUT, Finland.
URL: *https://urn.fi/URN:NBN:fi-fe2019090927472*

International Electrotechical commission (2022), *Industrial platinum resitance thermometers and platinum temperature sensors*, IEC 60751:2022 edn, International Electrotechical commission.

Kester, W. (2005), 'Which ADC architecture is right for your application?', *Analog Dialogue* **39**(2).
URL: *https://www.analog.com/media/en/analog-dialogue/volume-39/number-2/articles/the-right-adc-architecture.pdf*

Kester, W. (2008), *ADC Architectures III: Sigma-Delta ADC Basics*, Analog Devices. Tutorial MT-022, revision. A.
URL: *https://www.analog.com/media/en/training-seminars/tutorials/MT-022.pdf*

Kuglestadt, T. (2019), *Semiconductor Temperature Sensors Challenge Precision RTDs and Thermistors in Building Automation*, Texas Instruments. SNAA267A, Revision A.
URL: *https://www.ti.com/lit/an/snaa267a/snaa267a.pdf*

Kuisma, M., Immonen, A., Kyröläinen, H., Launis, E., Levikari, S., Peltonen, H., Pynnönen, M., Silvennoinen, M., Silventoinen, P. and Treves, L. (2019), Q-health - Lämpövuoanturin käyttö terveysteknologian ja liikunnan sovelluksissa. Loppuraportti, unpublished.

Laurila, H. (2017), *Thermocouple Cold (Reference) Junction Compensation*, Beamex.

Leens, F. (2009), 'An introduction to I2C and SPI protocols', *IEEE Instrumentation Measurement Magazine* **12**(1), 8–13.
URL: *https://doi.org/10.1109/MIM.2009.4762946*

Levikari, S., Immonen, A., Kuisma, M., Peltonen, H., Silvennoinen, M., Kyrolainen, H. and Silventoinen, P. (2020), 'Improving energy expenditure estimation in wearables using a heat flux sensor: First observations'.
URL: *https://arxiv.org/abs/2005.04054*

LMT70 (2015), *LMT70 datasheet*, Texas Instruments. Revision A.
URL: *https://www.ti.com/lit/ds/symlink/lmt70.pdf*

Maxim integrated (2000), *Comparing the I2C Bus to the SMBus*, Maxim integrated. Application note 476.
URL: *https://pdfserv.maximintegrated.com/en/an/AN476.pdf*

Maxim Integrated (2002), *The ABCs of ADCs: Understanding How ADC Errors Affect System Performance*, Maxim Integrated. Tutorial 748.
URL: *https://pdfserv.maximintegrated.com/en/an/AN748.pdf*

McNamara, A. (1962), 'Semiconductor diodes and transistors as electrical thermometers', *Review of scientific instruments* **33**(3), 330–333.
URL: *http://doi.org/10.1063/1.1717834*

NCP160 (2021), *NCP160 datasheet*, Onsemi. Revision 18.
URL: *https://www.onsemi.com/pdf/datasheet/ncp160-d.pdf*

Oudjida, A., Berrandjia, M., Liacha, A., Tiar, R., Tahraoui, K. and Alhoumays, Y. (2010), Design and test of general-purpose spi master/slave ips on opb bus, *in* '2010 7th International Multi- Conference on Systems, Signals and Devices', pp. 1–6.
URL: *https://doi.org/10.1109/SSD.2010.5585592*

Park, S. (1993), *Motorola Digital Signal Processors: Principles of Sigma-delta Modulation for Analog-to-digital Converters*, Motorola.

PCA9306 (2019), *PCA9306 datasheet*, Texas Instruments. Revision M.
URL: *https://www.ti.com/lit/ds/symlink/pca9306.pdf*

Pertijs, M. and Huijsing, J. (2006), *Precision temperature sensors in CMOS technology*, Springer.
URL: *https://doi.org/10.1007/1-4020-5258-8*

Rahikainen, H. (2021), Design and prototype of wearable data acquisition system, Master's thesis, Lappeenranta-Lahti University of Technology LUT, Finland.
URL: *https://urn.fi/URN:NBN:fi-fe2021092847306*

Santra, S., Guha, P. K., Ali, S. Z., Haneef, I. and Udrea, F. (2010), 'Silicon on insulator diode temperature sensor– a detailed analysis for ultra-high temperature operation', *IEEE sensor journal* **10**(5).
URL: *https://doi.org/10.1109/JSEN.2009.2037822*

Sapozhnikov, S., Mityakov, V. and Mityakov, A. (2020), *Heatmetry - The Science and Practice of Heat Flux Measurement*, Springer.
URL: *https://doi.org/10.1007/978-3-030-40854-1*

Schackmann, R. (2019), *Low-Power Design Techniques for Temperature-Sensing Applications*, Texas instruments. SNIA026.
URL: *https://www.ti.com/lit/an/snia026/snia026.pdf*

Sherry, B. (2003), *Chopping on* $\Sigma - \Delta$ *ADCs*, Analog Devices. Application note 609, revision 0.
URL: *https://www.analog.com/media/en/technical-documentation/application-notes/an-609.pdf*

Simunic, T., Benini, L., Glynn, P. and De Micheli, G. (2000), 'Dynamic power management for portable systems', *MobiCom '00: Proceedings of the 6th annual international conference on Mobile computing and networking* pp. 474–479.
URL: *https://doi.org/10.1145/345910.345914*

TCA9548A (2021), *TCA9548A datasheet*, Texas Instruments. Revision B.
URL: *https://www.ti.com/lit/ds/symlink/tca9548a.pdf*

TE (2018), *NTC thermistor sensor performance: Accuracy, Interchangeability, Beta Tolerance, Tolerance Comparison, Stability, Drift, and Moisture Induced Failure*, TE connectivity sensors. Revision 02/2018.
URL: *https://www.te.com/content/dam/te-com/documents/sensors/global/te-app-note-ntc-sensor-performance.pdf*

TE (2021), *THERMOPILE SENSOR FOR CONTACTLESS TEMPERATURE*, TE connectivity sensors. Application note, revision 01/2021.
URL: *https://www.te.com/content/dam/te-com/documents/sensors/global/analog-digital-thermopile-application-note.pdf*

Thomas, H. P. (1990), 'The international temperature scale of 1990 (ITS-90)', *Metrologia* **27**(1).
URL: *https://doi.org/10.1088/0026-1394/27/1/002*

TMP006 (2011), *TMP006 User's Guide*, Texas Instruments. Original revision.

TMP006 (2012), *TMP006 datasheet*, Texas Instruments. Revision C.

TMP117 (2019), *Precise Temperature Measurements With the TMP116 and TMP117*, Texas Instruments. SNOA986A, Revision A.
URL: *https://www.ti.com/lit/an/snoa986a/snoa986a.pdf*

TMP117 (2021), *TMP117 datasheet*, Texas Instruments. Revision C.
URL: *https://www.ti.com/lit/ds/symlink/tmp117.pdf*

Vittoz, E. A. and Olivier, N. (1979), 'A low-voltage CMOS bandgap reference', *IEEE Journal of solid-state circuits* **SC-14**(3).
URL: *https://doi.org/10.1109/JSSC.1979.1051218*

Wood, S., Mangum, B., Filliben, J. and Tillett, S. (1978), 'An investigation of the stability of thermistors', *J. RES. NATL. BUR. STAN.* **83**(3), 247.
URL: *https://doi.org/10.6028/jres.083.015*

Appendices

Appendix 1 Major uncertainty sources in the test setup

Table 1. Sensor accuracy according to manufacturer.

	Accuracy [°C]	Notes
TMP117	±0.1	
HDC2080	±0.4	
LMT70	±0.13	+ ADC
PT1000	±0.18	+ ADC
Reference PT1000	±0.05	+ ±0.18

Table 2. ADC reference uncertainty for LMT70 and PT1000.

	Initial accuracy		Temperature drift ΔT 35° C	
	Deviation [mV]	Sensor [° C]	Deviation [mV]	Sensor [° C]
Internal reference and LMT70	±5	±0.5	±1.3	±0.13
ADR130B and PT1000 WT bridge	±1.75	±0.27	±2.1	±0.33
PT1000 in 3-wire	Ratiometric			

Appendix 2 Sensor current consumption per measurement cycle

Sensor and ADC settings according to chapter 4.

Table 1. Average current consumption for 0.1 Hz measurement cycle.

	Current [μA]		Conversion time		Avg current [μA]	Notes
	On	Off	On [ms]	Off [s]		
TMP117	135	0.150	124	9.876 s	18.2	
HDC2080	550	50	0.610	9.999	1	
LMT70	9,2	0	200	9.8	1.84	+ ADC
PT1000	100	0	200	9.8	20	+ ADC
ADC	205	2	200	9.8	60	

Appendix 3 Digital board schematic

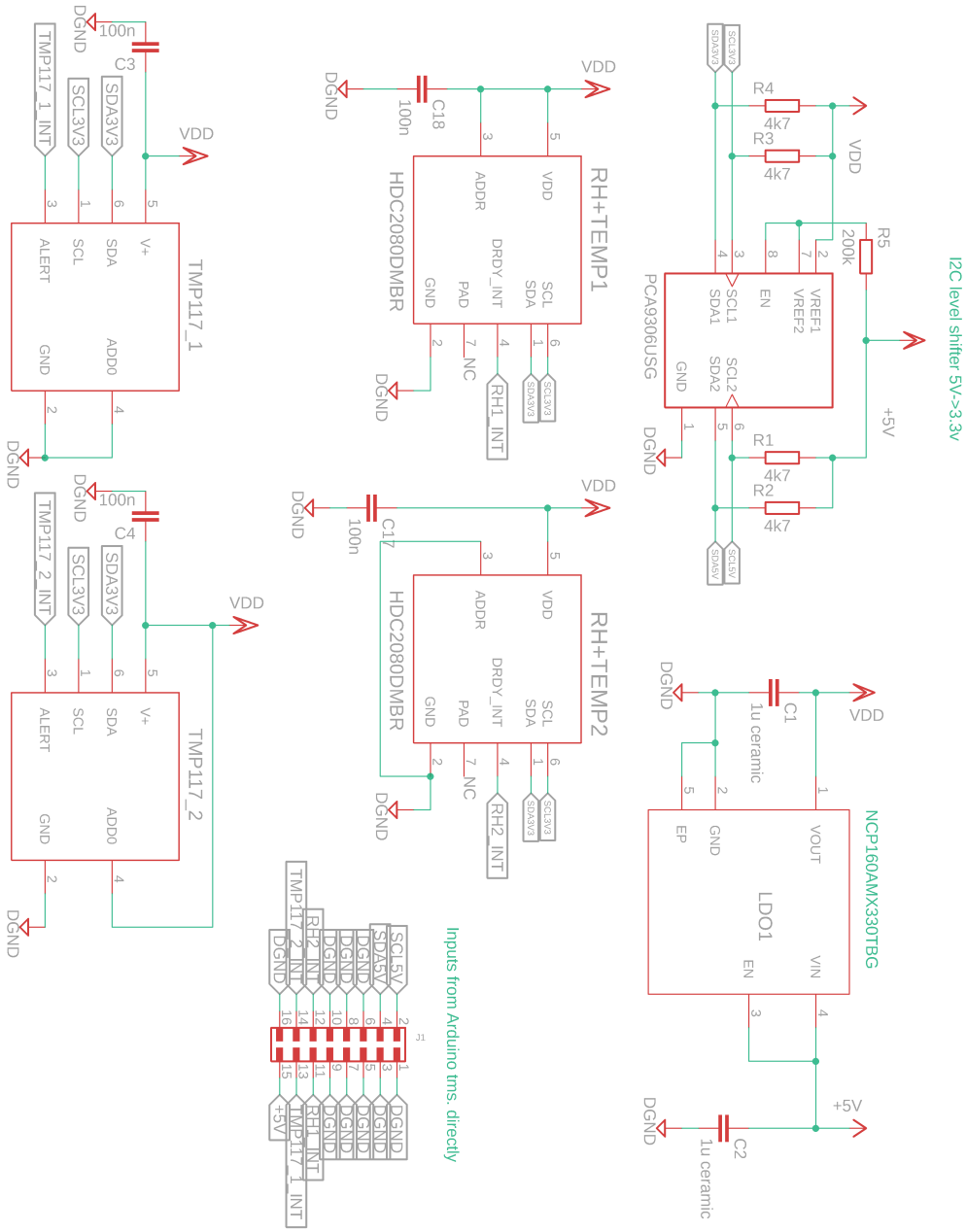

Appendix 4 ADC board schematic

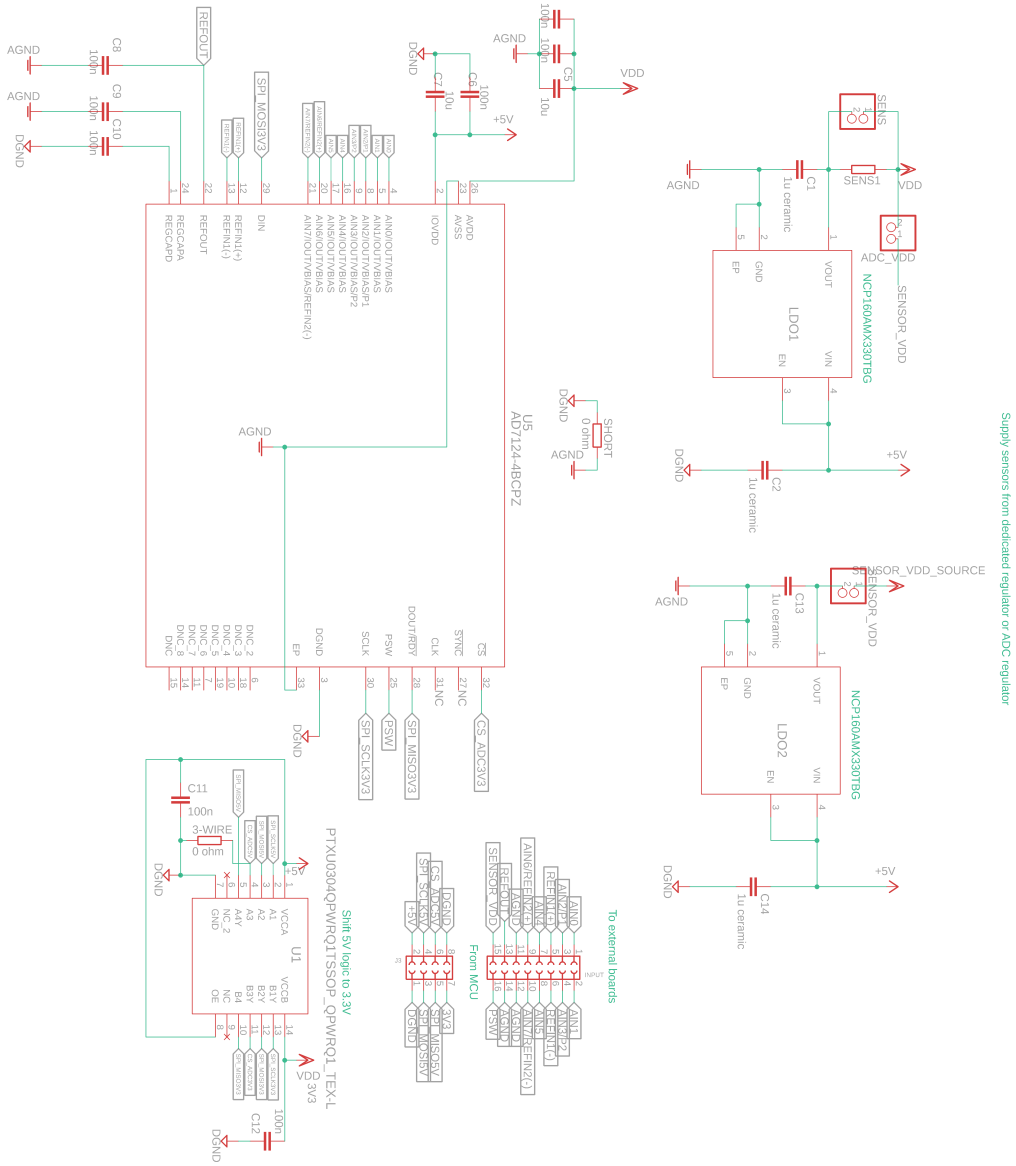

Appendix 5 LMT70 board schematic

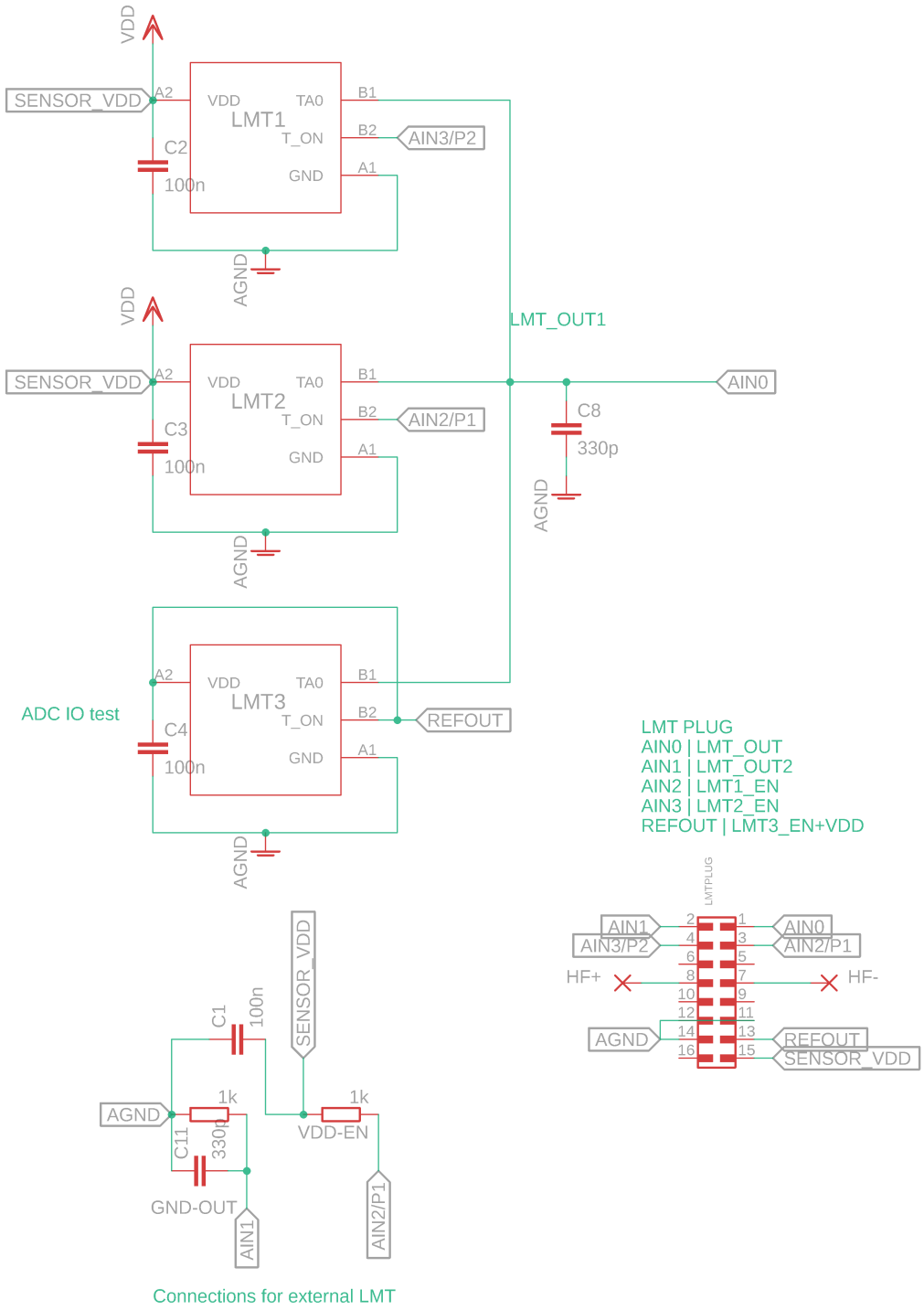

Appendix 6 PT1000 board schematic